The Leishmania donovani chaperone cyclophilin 40 is essential for intracellular infection independent of its stage-specific phosphorylation status.

Wai-Lok Yau, Pascale Pescher, Andrea Macdonald, Sonia Hem, Dorothea Zander, Silke Retzlaff, Thierry Blisnick, Brice Rotureau, Heidi Rosenqvist, Martin Wiese, et al.

The *Leishmania donovani* chaperone cyclophilin 40 is essential for intracellular infection independent of its stage-specific phosphorylation status

Wai-Lok Yau[1,2], Pascale Pescher[1], Andrea MacDonald[2], Sonia Hem[3], Dorothea Zander[2], Silke Retzlaff[3,+], Thierry Blisnick[4], Brice Rotureau[4], Heidi Rosenqvist[5,++], Martin Wiese[5], Philippe Bastin[4], Joachim Clos[2], and Gerald F. Späth[1,*]

Institut Pasteur and Centre National de la Recherche Scientifique URA 2581, [1]Unité de Parasitologie Moléculaire et Signalisation, and [4]Unité de Biologie Cellulaire des Trypanosomes, 25 rue du Dr Roux, F-75015 Paris, France; [2]Clos Group (Leishmanasis) and [3]Electron Microscopy Service, Bernhard-Nocht-Institut für Tropenmedizin, Bernhard-Nocht-Str. 74, D-20359 Hamburg, Germany; [3]Plate-forme de spectrométrie de masse protéomique - MSPP, Biochemie et Physiologie Moléculaire des Plantes, UMR 5004 CNRS/UMR 0386 INRA/Montpellier SupArgo/Université Montpellier II, F-34060 Montpellier, France; [5]Strathclyde Institute of Pharmacy and Biomedical Sciences, University of Strathclyde, Glasgow, Scotland, UK

* Correspondence: Gerald Späth
Institut Pasteur, 25 rue du Dr Roux, 75015 Paris, France
Phone: +33.1.40.61.38.58; Fax: +33.1.45.68.83.33
E-mail: gerald.spaeth@pasteur.fr

Short title: LdCyP40 null mutant analysis

Key words: *Leishmania donovani*, stress protein, cyclophilin 40, null mutant analysis, intracellular survival, chaperone phosphorylation

+current address: Altona Diagnostics, Moerkenstr. 12, 22767 Hamburg, Germany

++current address: Novo Nordisk, Novo Nordisk Park 1, DK-2760 Maaloev, Denmark

Summary

During its life cycle, the protozoan pathogen *Leishmania donovani* is exposed to contrasting environments inside insect vector and vertebrate host, to which the parasite must adapt for extra- and intracellular survival. Combining null mutant analysis with phosphorylation site-specific mutagenesis and functional complementation we genetically tested the requirement of the *Leishmania donovani* chaperone cyclophilin 40 (LdCyP40) for infection. Targeted replacement of LdCyP40 had no effect on parasite viability, axenic amastigote differentiation, and resistance to various forms of environmental stress in culture, suggesting important functional redundancy to other parasite chaperones. However, ultra-structural analyses and video microscopy of *cyp40-/-* promastigotes uncovered important defects in cell shape, organization of the subpellicular tubulin network and motility at stationary growth phase. More importantly, *cyp40-/-* parasites were unable to establish intracellular infection in murine macrophages and were eliminated during the first 24 hours post infection. Surprisingly, *cyp40-/-* infectivity was restored in complemented parasites expressing a CyP40 mutant of the unique S274 phosphorylation site. Together our data reveal non-redundant CyP40 functions in parasite cytoskeletal remodeling relevant for the development of infectious parasites *in vitro* independent of its phosphorylation status, and provides a framework for the genetic analysis of *Leishmania*-specific phosphorylation sites and their role in regulating parasite protein function.

Introduction

Parasitic protozoa of the genus *Leishmania* are the etiological agents of leishmaniases, severe human diseases with clinical manifestations ranging from self-curing cutaneous lesions to fatal visceral infection. During the infectious cycle, *Leishmania* replicate as extracellular flagellated promastigotes in the midgut of female phlebotomine sand flies where they undergo an environmentally triggered differentiation process termed metacyclogenesis to develop into highly infectious metacyclic promastigotes (Sacks *et al.*, 1984). Following transmission by blood feeding sand flies, metacyclic parasites are engulfed by phagocytes such as macrophages, where they differentiate into non-motile amastigotes that cause the pathology of the disease.

In vitro differentiation of infectious metacyclic parasites is induced by nutritional starvation or acidic pH, and development of amastigote-like cells in culture is triggered by pH and temperature change (Zakai *et al.*, 1998; Cunningham *et al.*, 2001; Barak *et al.*, 2005), suggesting that *Leishmania* stage-differentiation occurs through sensing of environmental stress signals encountered inside insect and vertebrate hosts (Zilberstein *et al.*, 1994). Recently, a role of stress signaling in parasite development has been suggested based on phosphoproteomics studies. Gel-based proteomics approaches comparing enriched phosphoprotein fractions from promastigotes and axenic amastigotes revealed a surprising divergence of the stage-specific phosphoproteome with more than 30% of proteins showing statistically significant differential phosphorylation (Morales *et al.*, 2008; Morales *et al*., 2010). Phosphorylation events in amastigotes were almost exclusively restricted to heat shock proteins and chaperones and occurred largely at parasite-specific phosphorylation sites (Hem *et al.*, 2010), suggesting regulation of the *Leishmania* response to stress by post-translational rather than classical transcriptional mechanisms. This possibility has been investigated previously for the stress-induced protein 1 (STI1), a chaperone that acts as a scaffolding protein for the assembly of foldosome complexes (Pratt and Dittmar, 1998). Null mutant analysis of STI1 in *L. donovani*

established the requirement of this protein for parasite survival *in vitro,* and complementation analysis by plasmid shuffle identified the two phosphorylation sites S15 and S481 as essential for STI1 function and parasite viability (Morales *et al*., 2010).

One group of stress proteins that showed increased phosphorylation in amastigotes in these studies is represented by immunophilins, a protein family that includes cyclophilins (CyPs) and FK506 binding proteins (FKBPs), which are characterized by a peptidyl-prolyl isomerase activity required for proper protein folding (Barik, 2006). In a previous study, we revealed stage-specific functions of cyclophilins using the CyP inhibitor cyclosporin A (CsA) (Yau *et al.*, 2010). Inhibitor-treated promastigotes underwent non-synchronous cell cycle arrest and acquired features similar to amastigotes, including oval shape and shortening of the flagella reminiscent of *L. donovani* promastigotes treated with the HSP90 inhibitor Geldanamycin (Wiesgigl and Clos, 2001). In contrast, treatment of axenic amastigotes resulted in parasite death, a phenomenon that was abrogated by temperature shift from 37°C to 26°C. While this pharmacological approach suggests potential roles of cyclophilins in parasite proliferation and thermotolerance and sheds new light on the stage-specific action of CsA and its lethal effects on intracellular *Leishmania* (Yau *et al.*, 2010), the pleiotropic inhibition of multiple cyclophilins and the phosphatase calcineurin by CsA-CyP complexes (Chappell and Wastling, 1992) raise questions about the specific function of each of the 17 *Leishmania* cyclophilins.

The effects of CsA on *L. donovani* differentiation and thermotolerance, its binding to parasite cyclophilin 40 (LdCyP40) (Yau *et al.*, 2010), and its stage-speific phosphorylation in the axenic amastigotes prompted us to assess the role of this co-chaperone and its modification in parasite survival and infectivity combining gene deletion, phosphoproteomics, and complementation approaches. CyP40 is a highly conserved bi-functional protein that carries peptidyl-prolyl isomerase (PPIase) activity and forms dynamic complexes in yeast and mammalian cells with HSP90 through its conserved tetratricopeptide repeat (TPR) domains

(Hoffmann and Handschumacher, 1995). The loss-of-function study presented here identifies important roles for LdCyP40 in the development of infectious parasites *in vitro* and intracellular parasite survival independent of its phosphorylation status, thus establishing a novel link between *L. donovani* chaperone activity and stress-induced parasite differentiation relevant for host cell infection.

Results

L. donovani CyP40 is constitutively expressed but stage-specifically phosphorylated.

CyP40 belongs to the immunophilin superfamily that comprises 17 members in *Leishmania* (Yau *et al*., 2010). We first investigated the domain structure and sequence conservation of this protein across trypanosomatid parasites (*L. major*, *L. infantum*, *L. braziliensis*, *T. brucei* and *T. cruzi*) and various higher eukaryotes, including human, mouse, cow, and yeast. The putative CyP40 protein sequences were retrieved from the UniProt (http://www.uniprot.org/) and TriTrypDB databases (http://tritrypdb.org/tritrypdb/) by Blast search using *L. major* cyclophilin 40 (LmjF35.4770) as a query and aligned using ClustalW 2.0.12. *Leishmania* CyP40 displays the characteristic two-domain structure (Fig. 1A). The N-terminal cyclophilin-like domain (CLD) spans 171 residues and is highly conserved showing 68.8% of amino acid identity across the analyzed organisms. This domain carries the enzymatic peptidyl-prolyl isomerase (PPIase) function and is the target of the cyclophilin-specific inhibitor cyclosporin (CsA). The functional residues for both PPIase activity and CsA binding are highly conserved as expected from our previously published observations that *L. donovani* CyP40 carries isomerase activity and can be enriched from crude parasite extracts by affinity chromatography using immobilized CsA (Yau *et al*., 2010). In addition, a cleft localized C-terminal of the CLD domain shows a series of conserved residues that have been previously implicated in CyP40 chaperone activity (Mok *et al.*, 2006). The C-terminal part of CyP40 contains three distinct TPR motifs that are

less conserved (50.4%, 47.3% and 50.2% of identity for TPR1, 2 and 3 respectively) and together form the TPR domain known to interact with the conserved EEVD consensus sequence of HSP70 and HSP90 (Ward *et al*., 2002). Together these data identify *Leishmania* CyP40 as a highly conserved member of the eukaryote immunophilin protein family that likely interacts with HSPs and carries chaperone function.

In our previous proteomics studies on the protein phosphorylation dynamics during *Leishmania* differentiation, *L. donovani* LdCyP40 abundance was significantly increased in the phosphoproteome of axenic amastigotes when compared to promastigotes, suggesting amastigote-specific phosphorylation of this protein (Morales *et al.,* 2008; Morales *et al.,* 2010). However, this putative stage-specific phosphorylation has not been validated in *bona fide* animal-derived amastigotes, and whether the increase of abundance results from an increase in phospho-stoichiometry or simply increased protein expression has not been investigated. To distinguish between these two possibilities, we analyzed LdCyP40 stage-specific expression and phosphorylation profiles by Western blotting using total protein extracts and phosphoprotein fractions enriched by immobilized metal affinity chromatography obtained from cultured promastigotes, axenic amastigotes, and *bona fide* amastigotes purified from *L. donovani* infected hamster spleen. As judged by α-tubulin expression used as normalization control, LdCyP40 is constitutively expressed across all stages tested, but shows a significant increase in abundance in the phosphoprotein fraction of axenic and hamster-derived amastigotes compared to promastigotes (Fig. 1B). The weaker signal observed in splenic amastigotes compared to axenic amastigotes may result from unequal loading or reflects a difference in phosphorylation levels between both samples. These results establish LdCyP40 stage-specific *de novo* phosphorylation and a substantial increase in the phospho-stoichiometry of this protein in amastigotes.

Establishment of cyp40-/- null mutants.

We established LdCyP40 null mutant parasites to study the biological functions of LdCyP40 and ultimately assess the physiological role of stage-specific CyP40 phosphorylation by complementation. The endogenous alleles were replaced using two targeting constructs comprising puromycin and bleomycin resistance genes flanked by the 5' and 3'UTRs of LdCyP40 (Fig. 2A and Fig. S1). Respective add-back controls re-expressing LdCyP40 from the ribosomal locus under the control of the CyP40 3'UTR were generated using a knock-in strategy (Fig. 2A and Fig. S2). The absence of the LdCyP40 ORF and corresponding protein in six independent null mutant clones and its re-expression in complemented parasites was confirmed by PCR (Fig. 2B and data not shown) and Western blot analysis (Fig. 2C and Fig. S3).

Morphological characterization of cyp40-/- null mutant and add-back clones.

Microscopic observation of the two independent null mutant clones *cyp40-/-* cl.4 and cl.5 and four independent add-back clones as well as add-back pools derived from each null mutant clone revealed important morphological alternations at stationary growth phase that correlated with the absence of CyP40 expression (Fig. S4A). At logarithmic growth phase, CyP40 null mutant promastigotes were morphologically identical to wild-type and add-back controls as judged by Giemsa staining of fixed parasite cultures (Fig. S4A, left panels). By contrast 70% of *cyp40-/-* cells at stationary growth phase of two independent null mutant clones acquired a small spherical cell shape, while wild-type parasites and add-back clones showed the spindle shaped cell body characteristic for stationary phase parasites (Fig. S4A, right panels). Moreover, measurements of cell body and flagellum length revealed a significant reduction of the ratio between both parameters in *cyp40-/-* cells (Fig. S4B). Given the reproducibility of this

phenotype, most of the subsequent experiments were performed with CyP40 null mutant clone 4 and its corresponding add-back pool if not otherwise stated.

As cell rounding is often associated with cellular stress and apoptotic cell death (Lee *et al.*, 2002; Gannavaram and Debrabant, 2012), we next investigated integrity and ultra-structural organization of CyP40 null mutant cells and controls. Wild-type, *cyp40-/-* and *cyp40-/-/+* promastigotes were fixed with 2% glutaraldehyde and analyzed by scanning electron microscopy (Fig. 3A). This analysis confirmed the atypical spherical cell shape of *cyp40-/-* stationary phase promastigotes and provided a first indication of their cellular integrity. Likewise, analysis by transmission electron microscopy revealed no overt alterations in cellular organization of *cyp40-/-* cells, which showed intact nuclei and mitochondria, and absence of apoptotic bodies or autophagosomes (Fig. 3B). Finally, direct assessment of cell death by FACS analysis following membrane exposure of phosphatidylserine with annexin V-FITC and exclusion of propidium iodide did not reveal any significant change in cell viability of stationary *cyp40-/-* parasites after 6 days of *in vitro* culture (Fig. 3C). Together these results rule out the possibility of cell death as the cause of *cyp40-/-* morphological alterations but rather suggest a defect in parasite development and cellular remodeling at stationary phase.

Phenotypic characterization of stationary phase cyp40-/- promastigotes.

During the infectious cycle, non-infectious procyclic promastigotes differentiate into highly infective metacyclic promastigotes in response to nutritional starvation after digestion and excretion of the blood meal. This process is mimicked in culture during stationary growth phase (Sacks *et al.*, 1984; da Silvaand Sacks, 1987) and is accompanied by the expression of characteristic biological and morphological markers, including expression of high molecular weight LPG and increase in SHERP mRNA abundance. The altered morphology of *cyp40-/-* parasites primed us to investigate the status of these phenotypic markers. First, monitoring cell

density of WT, *cyp40-/-* and add-back promastigotes with a CASY cell counter, deletion of CyP40 did not affect the rate of proliferation nor the density reached at stationary phase (Fig. 4A). Surprisingly, despite defects in stationary phase morphology, *cyp40-/-* promastigotes showed normal expression of higher molecular weight LPG characteristic for stationary phase parasites as revealed by Western blot analysis using the anti-LPG antibody CA7AE (Fig. 4B), and induced SHERP mRNA to levels corresponding to WT and add-back controls (Fig. 4C). Together these data demonstrate that *L. donovani* CyP40 is dispensable for parasite survival *in vitro* under standard culture conditions, and is not required for metacyclic-specific glycolipid remodeling or gene regulation, at least for the markers investigated here. To further characterize the stationary phase defect of *cyp40-/-* parasites, we investigated the functional properties of infectious, stationary phase parasites, including cell motility and intracellular survival.

CyP40 null mutants show reduced motility and a loosened subpellicular tubulin network.

An important functional characteristic of stationary phase parasites is a significant increase in motility, which is of physiological relevance in the natural setting for migration of metacyclic parasites from sand fly midgut to larynx (Walters *et al*., 1989; Walters *et al*., 1993), or the establishment of host cell infection (Uezato *et al*., 2005; Forestier *et al.*, 2011). We quantified motility in at least 741 WT, *cyp40-/-* and add-back promastigotes obtained from logarithmic and stationary phase cultures utilizing video microscopy and *in silico* tracking analysis. Qualitative observation of each movie did not reveal any significant difference in flagellar wave orientation and flagellar beating amplitude across all lines and both culture conditions (data not shown). Likewise, quantitative analysis showed no significant difference in beating frequencies and speed between WT, *cyp40-/-*, and add-back log phase promastigotes. As expected, WT and add-back promastigotes showed a statistically significant increase in motility

speed and flagellar beat frequency at stationary phase (Fig. 5A), and moved in a uni-directional way over extended distances (Fig. 5B and Video S1). By contrast, CyP40 null mutant parasites do not increase speed at stationary growth phase (Fig. 5A) and show a defect in directional motility as they largely spin on themselves (Fig. 5B and Video S1).

As judged by transmission electron microscopy, this motility defect was not caused by alterations in flagellar structure of *cyp40-/-* parasites, which maintained the characteristic 9+2 organization of the axoneme (Fig. 5C). However, investigating more closely the *Leishmania* subpellicular tubulin network by scanning EM after removal of the parasite plasma membrane by detergent treatment, stationary phase *cyp40-/-* promastigotes showed a significantly loosened tubulin network, in contrast to the very dense, small-meshed network observed in wild-type parasites (Fig. 5D). Western blot analysis of WT, *cyp40-/-* and add-back parasites from logarithmic and stationary cultures did not reveal any significant difference in expression levels of α- and β-tubulin, with the exception of a small β-tubulin isoform at around 33 kDa, which is specific for stationary phase cells and slightly reduced in CyP40 null mutants (Fig. S5). This finding was confirmed by quantitative proteomics using 2D-DIGE analysis of total extracts of WT and *cyp40-/-* promastigotes from stationary growth phase that identified the small β-tubulin isoform (LinJ.21.2240, spot 928) with a highly significant, four-fold reduction of abundance in the null mutant *cyp40-/-* (Fig. 5E and Fig. S6). This isoform corresponds to a previously described proteolytic cleavage product of β-tubulin with a molecular weight of about 34 kDa (Drummelsmith *et al.*, 2003). Similar low molecular weight isoforms have been identified in the stage-specific proteomes of *L. major* and *T. cruzi* metacyclic parasites (Parodi-Talice *et al.*, 2007; Mojtahedi *et al.*, 2008), but their biological significance in stage-specific remodeling of the tubulin network remains to be elucidated. Together these data demonstrate non-redundant CyP40 functions in cytoskeletal remodeling of the parasite during stationary

244 growth phase, which is likely the basis for the aberrant morphology and the motility defect
245 observed in *cyp40-/-* parasites.
246
247 *Leishmania cyp40-/- mutants fail to establish intracellular infection.*
248 The development of highly infectious metacyclic parasites can be mimicked by exposing
249 promastigotes to various forms of stress, including nutritional starvation and acidification at
250 stationary phase (da Silva and Sacks, 1987; Bate and Tetley, 1993; Zakai *et al*., 1998; Serafim
251 *et al*., 2012). The stationary phase-specific defects of *cyp40-/-* promastigotes primed us to
252 investigate their capacity to infect host cells. Bone marrow-derived macrophages obtained from
253 C57BL/6 mice were incubated for 2 hours with WT, *cyp40-/-*, and add-back stationary phase
254 promastigotes at a multiplicity of infection of 10 parasites per host cell, free parasites were
255 removed by washing, and intracellular parasite burden was determined by nuclear staining and
256 fluorescence microscopy at 2, 24, and 48 hours post infection. The *cyp40-/-* cells were
257 phagocytosed at levels comparable to the controls with 80% of macrophages hosting a mean of
258 2.5 parasites per infected host cell (Fig. 6A). While WT and add-back parasites persisted over
259 the 48 hours post infection period and showed intracellular proliferation as documented by the
260 increase in number of parasites per infected macrophage (Fig. 6A, lower panel), the level of
261 *cyp40-/-* infection was reduced by over 90% during the first 24 hours and parasites were
262 completely eliminated by 48 hours post infection (Fig. 6A). We next tested if intracellular
263 elimination of *cyp40-/-* parasites is caused by a susceptibility to elevated temperature or acidic
264 pH encountered inside the host cell, or results from a defect in amastigote differentiation.
265 CyP40 null mutant promastigotes grown at 37°C did not show any significant difference to WT
266 and add-back parasites (Fig. S7A), and axenic amastigotes developed and proliferated normally
267 in response to both temperature and pH shift as judged by cell counting (Fig. 6B) and
268 assessment of expression of the axenic amastigote marker protein A2 (Fig. 6C). Thus,

LdCyP40 carries essential functions for successful host cell infection independent of parasite resistance to acidic pH, elevated temperature, or amastigote development.

Functional assessment of CyP40 phosphorylation.

The failure of *cyp40-/-* parasites to establish intracellular infection provided an interesting read out to test for the function of CyP40 phosphorylation in parasite infectivity using complementation analysis. We investigated the CyP40 amino acid residues that were phosphorylated by using LC-ESI-MS/MS analysis. Axenic amastigote protein extracts from transgenic *L. donovani* over-expressing Strep::CyP40 were collected and Strep::CyP40 was enriched by affinity chromatography using streptactin agarose liquid chromatography (Fig. S8). After SDS-PAGE and Coomassie Brilliant Blue staining, the band corresponding to Strep::CyP40 was extracted and subjected to phosphopeptide analysis by LC-ESI-MS/MS. MS analysis revealed that residue serine 274 (S274) of CyP40 was the only detected phosphorylation site of CyP40 in axenic amastigotes (Fig. 7A and Fig. S9). The multiple sequence alignment of trypanosomatid CyP40 described in Fig. 1 localizes S274 to the center of the TPR motif 2 and shows that it is unique among trypanosomatids (Fig. 7B). An independent study also pointed out that S274 is phosphorylated in *L. mexicana* (Dr. Martin Wiese, University of Strathclyde, Glasgow, unpublished data). These data suggest that phosphorylation at S274 of CyP40 is *Leishmania*-specific and may have critical roles in parasite survival.

To study the relationship between CyP40 phosphorylation and parasite infectivity, an add-back line was generated expressing a serine 274 to alanine (S274A) phosphorylation site mutant version of CyP40 (Fig. 7C, left panel, and Fig. S10), which was subsequently tested for *in vitro* infectivity. We next assessed the accumulation of this mutant in the parasite phospho-protein fraction to test if elimination of S274 is sufficient to abrogate phospho-specific affinity

294 purification of CyP40. Total protein extracts and phospho-protein enriched extracts from WT
295 treated or not with lambda phosphatase, or add-back parasites expressing CyP40-S274A were
296 analyzed by western blotting using anti-CyP40 antibody and anti-α-tubulin antibody for
297 normalization of the signals. As expected, robust amounts of CyP40 were detected in the wild-
298 type phospho-protein extracts, and this signal was strongly reduced by phosphatase treatment
299 prior to enrichment representing background levels of CyP40 enrichment likely due to non-
300 specific binding to the affinity matrix (Fig. 7C, right panel). The same level of background
301 signal was obtained with CyP40-S274A confirming that this residue represents the only
302 phosphorylation site in CyP40.

303 Bone marrow-derived macrophages were then infected with *cyp40-/-* promastigotes
304 complemented with CyP40-S274A. The controls, WT, *cyp40-/-* and add-back promastigotes
305 behaved in a similar fashion as described previously (Fig. 7D). The higher counts of infected
306 macrophage obtained with WT parasites compared to add-back control may be due to batch-to-
307 batch variation of parasites. The *cyp40-/-/+S274A* add-back promastigotes entered
308 macrophages and established infection at similar efficiency. The parasite number decreased in
309 the first 24 hours post infection but parasites started to multiply after 48 hours (Fig. 7D, left
310 panel). The intracellular proliferation of CyP40-WT and CyP40-S274A add-back did not show
311 any significant difference, as indicated by the number of parasites per 100 macrophages at 48
312 hours post infection (Fig. 7D, right panel). These data indicate that phosphorylation of CyP40
313 is either not important for the function of CyP40 in *Leishmania* intracellular survival, or can be
314 compensated by other co-chaperones.
315
316

Discussion

The conserved co-chaperone CyP40 participates in the formation of highly dynamic heat shock protein complexes across various eukaryotes (Pratt *et al.*, 2004; Ratajczak *et al*., 2003; Riggs *et al*., 2004; Pearl and Prodromou, 2006), and has been linked to many tissue- and organism-specific functions, including steroid receptor signaling in mammalian cells and yeast (Ratajczak *et al.*, 2009), or microRNA activity and assembly of RNA-induced silencing complexes (RISCs) in plants (Smith *et al.*, 2009; Ilki *et al*., 2012). No information is available on how this co-chaperone affects viability and infectivity of trypanosomatid pathogens, including *Leishmania*, even though parasite differentiation is triggered by environmental stress signals (Zilberstein and Shapira, 1994), has been previously linked to the formation of heat shock complexes (Morales *et al*., 2010), and is regulated by HSP90 activity (Wiesgigl and Clos, 2001). Here by utilizing a targeted null mutant approach we reveal non-redundant and essential CyP40 functions in *Leishmania* stage-specific morphogenesis, motility, and the development of infectious-stage parasites.

We recently obtained first insight into the biological roles and functional diversity of *L. donovani* CyPs and FKBPs using a pharmacological approach. Treatment of *L. donovani* promastigotes and axenic amastigotes with CsA and FK506 revealed important, redundant functions of CyPs and FKBPs in promastigote proliferation and morphogenesis, but unique function of *Leishmania* CyPs in parasite thermotolerance (Yau *et al*., 2010). The direct enrichment of CyP40 from *L. donovani* extracts using immobilized CsA, the presence of a conserved TPR domain in this protein, and its stage-specific phosphorylation in axenic amastigotes (Morales *et al*., 2008; Morales *et al*., 2010) suggested important stress functions of CyP40 in *Leishmania* differentiation and thermotolerance that may be regulated at post-translational levels.

However, the CyP40 loss-of-function analysis performed in this study shed a substantially different light on the protein's unique functions. In contrast to CsA treated promastigotes that underwent non-synchronous cell cycle arrest at logarithmic growth phase and showed morphological changes reminiscent of axenic amastigotes, i.e. retraction of the flagellum and oval cell body (Yau *et al*., 2010), *cyp40-/-* promastigotes did not show any overt defects in cell growth or cell shape at this culture stage. Moreover, absence of CyP40 expression did neither alter the IC50 to CsA nor did it affect the phenotypic response to this inhibitor (Fig S7 and data not shown) suggesting that CyP40 is not a major target of CsA at this culture stage. Finally, *cyp40-/-* parasites did not show any overt defects in resistance to various forms of stress, including nutritional starvation, acidic pH and elevated temperatures (Fig. 6D and S7), while CsA-treated parasites underwent cell death at 37°C (Yau *et al*., 2010). Thus, in contrast to other TPR domain containing chaperones in *Leishmania*, such as STI1 (Morales *et al*., 2010; Hombach *et al*., 2013) or SGT (Ommen *et al*., 2010), which are both essential for *Leishmania* promastigote viability, CyP40 carries non-essential functions at this stage, which may be redundant to other PPIases of the CyP or FKBP protein families and thus compensated in the null mutant.

Various aspects of the *cyp40-/-* null mutant phenotype pointed at essential and non-redundant CyP40 functions that were not observed during CsA treatment and thus are likely independent of the CyP40 PPIase activity targeted by this inhibitor (Yau *et al*., 2010). First, lack of CyP40 expression caused important morphological and structural alterations of stationary phase parasites, which adopted a rounded rather then characteristic needle-shaped morphology. These defects were linked to a loosening of the subpellicular tubulin network that determines parasite morphology and provides the rigidity necessary for efficient motility (Seebeck *et al*., 1990). These results point to unique CyP40 functions in regulating *Leishmania* cytoskeletal dynamics. Microtubule elongation and shortening are highly dynamic events that

366 are regulated by stabilizing or destabilizing interactions (Walczak, 2000). Recently, a role of
367 the CyP40 related immunophilin FKPB52 in regulating microtubule depolymerization through
368 direct interaction with tubulin via its TPR domain has been described in rat brain (Chambraud
369 *et* al., 2007). Given the capacity of CyP40 and FKBP52 to compete for molecular partners
370 (Ratajczak *et al.*, 2003), it is possible that CyP40 interacts with microtubules and promotes
371 tubulin polymerization to counteract FKBP52-mediated depolymerization. Alternatively, the
372 requirement of CyP40 for *Leishmania* morphological integrity at stationary growth phase may
373 be indirect and caused by misfolding of client proteins that require CyP40 co-chaperone
374 function. In yeast, TPR-domain containing co-chaperones make distinct and extensive contacts
375 with HSP90 that lead to a differential modulation of HSP90 chaperone function (Ratajcak *et* al.,
376 2009). For example, displacement of STI1 from HSP90 by the yeast CyP40 homolog CPR6
377 restores ATPase activity (Pearl and Prodromou, 2006). Based on our previous observation that
378 *L. donovani* STI1 acts as a scaffolding protein to assemble highly dynamic heat shock
379 complexes (Morales *et al.,* 2010), it is possible that lack of CyP40 alters the formation and
380 activity of foldosome complexes causing the observed phenotypic consequences of CyP40
381 deletion.

382 Second, *cyp40-/-* parasites showed an important, stage-specific defect in directional
383 motility despite integrity of the 9+2 structure of the axoneme. The presence of trypanosomatid
384 CyP40 in the flagellar proteome (Oberholzer *et al*., 2011) indicates that LdCyP40 may directly
385 interact with motor components for proper folding. This possibility is supported by various
386 studies of related FKBPs showing (i) direct interaction between the FKBP52 PPIase domain
387 and the motor protein dynein via dynamitin (Silverstein *et al*., 1999; Galigniana *et al*., 2001;
388 Galigniana *et al.,* 2004); (ii) an essential role of FKBP52 for sperm tail development and
389 movement (Hong *et al*., 2007); and (iii) a requirement of FKBP12 in *Trypanosoma brucei*
390 motility (Brasseur *et* al., 2013).

Finally, the most striking loss-of-function phenotype of *cyp40-/-* parasites is represented by the abrogation of intracellular parasite survival. Unfortunately the *L. donovani* strain used in our analysis failed to establish hamster infection (Fig. S11) likely due to a non-specific loss of virulence that occurs during parasite culture adaptation (Pescher et al, 2011). While we cannot rule out that loss of intracellular survival reflects a developmental defect caused by the morphological and cytoskeletal alterations observed at stationary phase culture, our observations that null mutant parasites are normal in viability and metacyclic marker expression, and convert normally into axenic amastigotes may point to different possible scenarios. Intracellular killing of *cyp40-/-* mutants may be associated with the requirement of LdCyP40 co-chaperone activity for proper folding of parasite survival factors, which may confer parasite resistance to macrophage cytolytic activities. Alternatively, the identification of LdCyP40 in the parasite secretome (Silverman *et* al., 2008) opens the possibility that this co-chaperone may directly interact with host phagolysosomal or cytoplasmic proteins to subvert host cytolytic activities and favor intracellular parasite survival, a scenario reminiscent to secreted *T. cruzi* CyP19, which inactivates the anti-microbial peptide trialysin of the reduviid insect vector by direct binding (Kulkarni *et al.*, 2013). A third possibility is the involvement of CyP40 in the sorting of exosome payload proteins, similar to the role played by the chaperone HSP100 (Silverman *et al.*, 2010). This idea would be supported by the very similar phenotypes of CyP40 (this paper) and HSP100 null mutants (Krobitsch and Clos, 1999).

In previous phosphoproteomics investigations we identified LdCyP40 as a major amastigote-specific phosphoprotein and revealed a coordinated increase in phosphorylation of all major parasite chaperones and HSPs during axenic amastigote differentiation, which occurred largely at parasite-specific sites (Morales *et al*., 2008; Morales *et al*., 2010; Hem *et al*., 2010). These results are compatible with the hypothesis that *Leishmania* stress protein function is regulated at post-translational levels through phosphorylation by stress-activated protein

kinases, a possibility that is supported by the genetic validation of two phosphorylation sites in *L. donovani* STI1 that are essential for parasite viability (Morales *et al*., 2010). The failure of *cyp40-/-* parasites to establish intracellular infection provided a powerful read out to further test this hypothesis and to assess the physiological role of CyP40 phosphorylation by site-directed mutagenesis of the single CyP40 phosphorylation site. Surprisingly, although CyP40 phosphorylation at S274 was highly stage-specific and observed exclusively in axenic and *bona fide* splenic amastigotes, expression of an LdCyP40 S274A mutant fully restored intracellular survival of *cyp40-/-* parasites thus ruling out an essential role of this modification in intracellular infection *in vitro*. The biological function of this highly conserved phosphorylation site eludes us. Phosphorylation of FKBP52 disrupts the binding activity of this chaperone to HSP90 and thus is required for the dynamic turnover of heat shock complexes (Miyata *et al*., 1997). The S274 CyP40 phosphorylation site maps to the TPR2 subdomain and thus may play a similar role in regulating the dynamics of protein-protein interactions, but may not cause a discernible phenotype due to the expression of other, functionally redundant TPR-domain proteins in *Leishmania.*

In conclusion, null mutant analysis of LdCyP40 revealed important non-redundant functions of this co-chaperone in parasite morphogenesis, cytoskeletal remodeling during stationary growth phase, motility, and infectivity. How LdCyP40 carries out its parasite-specific functions, and whether they depend on CyP40 isomerase and/or (co-)chaperone activities remains to be elucidated. In other organisms, CyP40 exerts its function mainly through binding to HSP90 (Li *et al.*, 2011). There are several lines of evidence that CyP40 functions in *Leishmania* may not follow this established model as isolation of HSP90 complexes by anti-STI1 immuno-precipitation from *L. donovani* promastigotes and axenic amastigotes did not reveal LdCyP40 (Morales *et al.*, 2010), although both co-chaperones can bind HSP90 simultaneously in other organisms (Li *et al.*, 2011). In addition, while the

LdCyP40 PPIase domain is highly conserved, the TPR domain underwent substantial evolutionary modification (Yau *et al.*, 2010), which may impact on LdCyP40-HSP interactions. Future studies applying structure/function analyses to assess LdCyP40 isomerase and chaperone activities, combined with pull down assays and native electrophoresis, will elucidate the roles of the LdCyP40 PPIase and TPR domains in *L. donovani* differentiation, virulence and stress protein interaction.

Experimental procedures

Ethics statement. All animals were handled according to institutional guidelines of the Central Animal Facility of the Institut Pasteur (Paris, France) and experiments were performed in accordance with protocols approved by the animal Experimentation Ethics Committee of the Institut Pasteur (permit #03–49) and the veterinary service of the French Ministry of Agriculture (number B-75-1159, 30 May 2011). The animals were housed and handled in accordance with good animal practice as defined by FELASA (www.felasa.eu/guidelines.php).

Mice, macrophages and parasites. Wild-type C57BL/6 mice were purchased from Charles River, and were kept and treated according to the institutional guidelines for animal experiments. Bone marrow-derived macrophages (BMMs) were prepared from the femurs of 6 – 8 weeks old female mice as described (Forestier *et al.*, 2011). *Leishmania donovani* strain 1SR (MHOM/SD/62/1SR) was maintained at 25°C, pH 7.4 in supplemented M199 medium (Kapler *et al.*, 1990; Hubel *et al.*, 1997). Axenic differentiation of promastigotes was performed as described (Goyard *et al.*, 2003; Morales *et al.*, 2008).

Multiple sequences analysis. The putative cyclophilin 40 protein sequences of human, mouse, bovine, yeast and several trypanosomatids, including *L. major*, *L. infantum*, *L. braziliensis*, *T. brucei* and *T. cruzi*, were retrieved from the NCBI (http://www.ncbi.nlm.nih.gov/protein/) and TriTrypDB databases (http://tritrypdb.org/tritrypdb/) by Blast search with algorithum blastp using *L. major* cyclophilin 40 (LmjF35.4770) as a query. The retrieved sequences were aligned with ClustalW 2.0.12 using the built-in programs of Geneious version 4.8 (Larkin *et al*., 2007; Kearse *et al*., 2012; http://www.geneious.com). Matrix Blosum62 was applied as the scoring rule for amino acid substitution (Henikoff and Henikoff, 1993). Sequence alignments with Expect (E) values less than 10^{-5} were considered significant.

Generation of *L. donovani cyp40-/-* mutants by gene replacement. Null mutant parasites were generated by sequential replacement of the endogenous *CYP40* alleles using two targeting constructs comprising puromycin and bleomycin resistance genes flanked by approximately 1000 bp of the 5' and 3'UTRs of the *L. infantum CYP40* gene (GeneDB accession number LinJ.35.4830) that were PCR amplified from *L. infantum* genomic DNA (strain MHOM/FR/91/LEM2259). Genomic DNA of parasites was extracted with Gentra Systems Puregene Tissue Core Kit A (Qiagen) according to the manufacturer's instruction.

For subsequent cloning of the 5'UTR, primer pairs CYP40-5'UTR-fwd (GGGGAATTCATTTAAATGAGATGCGGTAGATGTCCTG) and CYP40-5'UTR-rev (GGGGGTACCTGCGTGCGTGTAGGTCTAC) added EcoRI and SwaI sites (underlined) to the 5'-end, and a KpnI site to the 3'-end. For cloning of the 3'UTR, primer pairs CYP40-3'UTR-fwd (GGGGGATCCGTTGCGCCTGCCGGACAGAAC) and CYP40-3'UTR-rev (CCCAAGCTTATTTAAATGAGTGAGACGTGCACGCAAC) added BamHI site to the 5'-end, and HindIII and SwaI sites to the 3'-end. The amplified fragments were digested with EcoRI/KpnI and BamHI/HindIII and ligated into pUC19 vector digested with the same enzyme pairs yielding the constructs pUC-CYP40-5'UTR and pUC-CYP40-3'UTR. Next, the cloned 5'UTR fragment was liberated by EcoRI and KpnI digestion, ligated into pUC-CYP40-3'UTR digested with the same enzyme pair yielding the construct pUC-CYP40-5'3'UTR. For the construction of the final targeting constructs, the antibiotic resistance genes *PAC* and *BLE* were isolated from pUC-PAC and pUC-BLE after digestion with KpnI and BamHI and ligated into pUC-CYP40-5'3'UTR digested with the same enzymes, yielded the final constructs pUC-CYP40-5'PAC3' and pUC-CYP40-5'BLE3' used for *Leishmania CYP40* gene replacement.

For genetic complementation of the CyP40 null mutant, an "add-back" line was established using a knock-in strategy. The *CYP40* open reading frame was PCR amplified using

primers CYP40-5'Kpn (GGGGGTACCATGCCGAACACATACTGC) and CYP40-3'BglII (GGGAGATCTTCACGAGAACATCTTCTTG), adding KpnI and BglII sites (underlined) to the 5'- and 3'-ends of the *LmCYP40,* respectively. The amplified fragment was digested with these enzymes, ligated into pUC-CYP40-3'UTR digested with KpnI and BamHI yielding the construct pUC-CYP40+3'UTR. The cloned CYP40+3'UTR was liberated by digestion with Acc65I and SwaI, the 5'-protruding end of the digested fragment was filled-in with Klenow fragment, and cloned into XbaI/BglII digested and blunt ended vector pIRmcs3+ (Hoyer *et al.*, 2004) yielding the final construct pIR-CYP40 used for integration into the small ribosomal subunit (SSU) locus of the *cyp40-/-* genome.

The plasmids were extracted from transformed *E. coli* DH5α, purified using CsCl continuous gradient centrifugation and linearized with SwaI. The targeting fragments were separated by agarose electrophoresis, purified and transfected into logarithmic promastigotes by electroporation as described (Spath *et al.*, 2000; Ommen *et al.*, 2009). Integration of gene replacement constructs was verified by PCR using the primer pairs: (P1, CATTTGGCGCTTTTCATGC; P2, ATTACATCAGACGTAATCTG; P3, TGGAAAGTGCTACCCTGGTACGTC; P4, GTGGGCTTGTACTCGGTC; P5, GGAACGGCACTGGTCAAC). PCR products were analyzed by agarose gel electrophoresis.

Site-directed mutagenesis. Cloned *L. major CYP40* in the construct pUC-CYP40+3'UTR was used as template for site-directed mutagenesis that is based on a modified PCR (Hombach *et al*., 2013). The template was amplified by PCR using the following phosphorylated oligonucleotide pairs (mutation sites were underlined) to introduce the mutation: CYP40-S274A-fwd (GCAGTGGGCGGAGGCTCGCCACACGGCGTC) and CYP40-S274-rev (TGGAGCTTGATGGCGCACATTG). The PCR products were ligated and used to transform

competent *E. coli* DH5α (Invitrogen). Plasmids were extracted and purified for DNA sequencing to verify the mutation.

Cell counting. The cell density of parasite cultures were determined every 24 hours either using a CASY cell counter (Schärfe System) or microscopically by counting 2% (w/v) glutaraldeyhde fixed cells loaded into a Neubauer-improved cell counting chamber (Marienfeld).

Macrophage infection assays. Isolation and differentiation of BMMs were performed as described (Forestier *et al.*, 2011). The mature BMMs were treated with 20 mM EDTA for detachment. The dislodged cells were resuspended in complete RPMI medium and plated overnight in 24-well plates containing sterile 12-mm glass coverslips at a cell density of 1×10^5 cells/well. *L. donovani* promastigotes cultured for 6 days until stationary-phase ($8 - 10 \times 10^7$/ml), or axenic amastigotes from logarithmic growth phase ($1 - 5 \times 10^7$/ml) were washed three times with plain RPMI medium and once with infection medium (0.7% BSA, 25 mM HEPES [pH 7.4] in plain RPMI medium), incubated with BMMs at 37ºC with 5% CO_2 for 2 hours at a multiplicity of infection of 10 parasites per host cell. Extracellular parasites were then removed by washing the coverslips extensively with PBS and transfer of the cover slip into new 24-well plates containing 1 ml of fresh complete RPMI medium per well. This washing procedure was repeated daily until 5 days post infection. The plates were incubated for up to 5 days at 37ºC with 5% CO_2 during the experiment.

Analysis of intracellular parasite burden. Coverslips of quadruplicate experiments were collected at 0, 24 and 48 hours post infection, washed once with PBS and then fixed with 4% (w/v) paraformaldehyde for 15 min at room temperature. After three further washes with PBS

548 and one wash with ddH_2O, the coverslips were mounted with Mowiol medium containing
549 nuclear dye Hoechst 33342 (Invitrogen). At least 100 macrophages were imaged per coverslip
550 using Axioplan 2 wide field light microscope with the Apotome module (Carl Zeiss). Number
551 of parasites and macrophages was estimated counting host cell and parasite nuclei using ImageJ
552 (National Institute of Health, US) using a predefined pixel range for each cell type (400 to
553 infinity pixels, macrophages; 0 to 150 pixels, parasites; 100 to 200 pixels, CFSE labeled
554 parasites in case of mixed infection assay).
555
556 **Microscopic analyses.** *Giemsa staining analysis.* Parasites (1×10^6) were settled on poly-L-
557 lysine coated glass slides and air-dried overnight. The dried cells were fixed with methanol and
558 stained with Giemsa solution (Sigma) for 10 min. After rinsing with water and air-drying, the
559 slides were mounted with Immersol 518N (Carl Zeiss) and observed under an Axioplan 2 wide
560 field light microscope (Carl Zeiss). The acquired images were analyzed by Zeiss Axiovision
561 release 4.7 (Carl Zeiss) or Openlab v3.0 (Improvision).
562 *Scanning electron microscopy.* Parasites were washed twice in ice-cold PBS and then
563 fixed with 2% (w/v) glutaraldehyde (Sigma) in PBS with 0.1 M sodium cacodylate (pH 7.2).
564 Briefly, the fixed cells were treated with 1% (w/v) OsO_4 and dehydrated followed by critical-
565 point drying (CPD 7501, Polaron) and coated with gold powder (Ion Beam Coater 681, Gatan).
566 Samples were visualized with scanning electron microscope SEM 500 (Philips). For
567 cytoskeleton analysis, cells were treated with 1% Triton X-100 at 4ºC in PBS for 10 minutes to
568 strip the plasma membrane and visualize the cytoskeleton. The samples were then washed
569 twice in PBS, fixed in glutaraldehyde and processed for scanning electron microscopy in
570 standard conditions as described (Absalon *et al.*, 2008).
571 *Transmission electron microscopy.* Parasites were washed twice in ice-cold PBS and
572 then fixed with 2% (v/v) glutaraldehyde (Sigma) in PBS with 0.1 M sodium cacodylate (pH

7.2). The fixed cells were post-fixed in 1% (w/v) OsO_4 and then dehydrated with increasing ethanol concentrations (70–100%) and embedded in EPON epoxy resin (Hexion Speciality Chemicals). Ultrathin sections (~70 nm) were prepared using an Ultramicrotome (Ultra Cut E; Reichert/Leica) and stained with uranyl acetate and lead citrate. Sections were analyzed using the Tecnai Sprit TEM (FEI).

Annexin V-FITC assay. Parasites (2×10^7 cells) were washed and resuspended in 100 µl of binding buffer containing 100 µg/ml of FITC conjugated annexin V (a gift from Dr. Aude Foucher, Photeomix, Paris), 1 µg/ml of PI, 10 mM HEPES (pH 7.4), 140 mM NaCl and 5 mM $CaCl_2$. The suspensions were incubated at room temperature for 10 min in the dark. The stained cells were subjected to FACS analysis (λ_{ex} = 488 nm; λ_{em} = 515 nm [FITC] and 617 nm [PI]) with a FACSCalibur™ (BD Biosciences). 10,000 events were analyzed using FlowJo 8.7 (Tree Star).

SYBR Green-based semi-quantitative RT-PCR. SHERP cDNA was amplified using forward primer CGACAAGATCCAGGAGCTGAAGGAC and reversed primer CCTTGATGCTCTCAACCGTGCTG). Beta actin cDNA was amplified as reference gene to calculate relative expression levels of SHERP mRNA.

Motility analysis. For each condition, at least 3 movies were recorded (500 frames at 33 ms of exposure for 16 s movies). Samples were observed in their respective culture media (cell density of about 5×10^6 cells/ml in logarithmic phase or 10^7 cells/ml in stationary phase) under a 10× objective of an inverted DMI4000 microscope (Leica). Cells were filmed using a numeric camera Photometrics Evolve 512 (Photometrics). Movies were converted with the MPEG Streamclip V1.9b3 software (Squared 5) and analyzed with the ICY software

(http://www.bioimageanalysis.org/). For each movie, at least 255 cells were simultaneously tracked *in silico*. Mean speeds (in μm/s) were calculated from instant velocity data transferred and compiled in Microsoft Excel. Statistical analyses were performed in the KaleidaGraph V4.0 software (Synergy Software). Data were first filtered (number of spot detections > 3 and mean speed < 100 μm/s) to exclude false tracks (non-*Leishmania* objects, dead cells and/or attached cells). An ANOVA test was then performed with Tukey ad-hoc post-tests at 0.5 for intergroup comparisons ($p < 0.0001$).

***Leishmania* phosphoprotein enrichment.** Promastigotes, axenic amastigotes, and splenic amastigotes derived from *Leishmania* infected hamsters, were centrifuged at 1000 × g at 4ºC for 10 min. Pellets were washed twice with plain M199 medium, then resuspended in lysis buffer (150 mM NaCl, 50 mM Tris-HCl pH 7.4, 1% Triton X-100, 1% benzonase, and protease inhibitor cocktail [Roche]) and lysed at 4ºC for 30 min with vortexing every 10 min. The lysate was then sonicated on ice for 5 min (10 seconds pulse with a 20 seconds pause) using Bioruptor (Diagenode). Cell debris was removed by brief centrifugation. Protein concentration of lysates was estimated by RC DC protein assay (Bio-rad) and adjusted to 0.1 mg protein/ml with lysis buffer. Phosphoprotein was enriched using the Phosphoprotein purification kit (Qiagen) according to the manufacturer's instructions. Briefly, 2.5 mg of total protein were loaded to the equilibrated columns. Unbound proteins were removed by washing the column with 6 ml of lysis buffer. Bound phosphorylated proteins were eluted with 2 ml elution buffer and concentrated using Amicon Ultra-0.5 ml centrifugal filters with Ultracel® 10K membrane (Millipore).

Phosphopeptide identification. Cell lysate extracted from transgenic *L. donovani* expressing Strep::CyP40 (refer to supporting information) was separated by SDS-PAGE. Separated

Strep::CyP40 was trypsin-digested and diluted in loading buffer (80% ACN, 5% TFA). The sample was then processed for LC-ESI-MS/MS analysis to identify phosphorylation sites, as described (Morales *et al*., 2010). Briefly, digested protein was diluted in loading buffer (80% ACN, 5% TFA) and loaded on TiO_2 microcolumns. After two washing steps in 10 µl loading buffer and 60 µl buffer 2 (80% ACN, 1% TFA), phosphopeptides were eluted using 10 µl NH_4OH (pH 12), dried, then resuspend in 10 ul of 0.1% formic acid before analyzing with a Q-TOF mass spectrometer (Maxis; Bruker Daltonik GmbH, Bremen, Germany), interfaced with a nano-HPLC U3000 system (Thermo Scientific, Waltham, USA). Samples were concentrated with a pre-column (Thermo Scientific, C18 PepMap100, 300 μm × 5 mm, 5 μm, 100 A) at a flow rate of 20 µL/min using 0.1% formic acid. After pre-concentration, peptides were separated with a reversed-phase capillary column (Thermo Scientific, C18 PepMap100, 75 μm × 250 mm, 3 μm, 100 A) at a flow rate of 0.3 µL/min using a two-step gradient (8 % to 28 % acetonitrile in 40 min then 28 % to 42 % in 10 min), and eluted directly into the mass spectrometer. Proteins were identified by MS/MS by information-dependent acquisition of fragmentation spectra of multiple charged peptides and MS/MS raw data were analysed using Data Analysis software (Bruker Daltonik GmbH, Bremen, Germany) to generate the peak lists. The *L. major* database from GeneDB was searched using MASCOT software (Matrix Science, London, UK) with the following parameters: trypsin cleavage, one missed cleavage sites allowed, carbamidomethylation set as fixed modification, 10 ppm mass tolerance for MS, and 0.05 Da for MS/MS fragment ions. Phosphorylation (ST), Phosphorylation (Y) and oxidation (M) were allowed as variable modifications. All phosphorylated peptides were first checked for the presence of the major fragment ion $[MH-H_3PO_4]+ = MH - 98$ Da corresponding to the loss of the phosphate moiety and identified positively by MASCOT. In addition, all MS/MS spectra were carefully checked manually for assignment of phosphorylation sites.

Western blot analysis. Samples in 1 × Laemmli buffer were separated by 10% SDS-PAGE and then transferred to PVDF membranes. Rabbit anti-CyP40 antiserum (1:20000 dilution, Yau *et al.*, 2010), mouse anti-A2 antibody (clone C9, 1:50 dilution, Zhang *et al.*, 1996), mouse anti-LPG antibody (clone CA74E, 1:20000 dilution, Tolson *et al.*, 1994), mouse anti-α-tubulin antibody (clone B-5-1-2, 1:20000 dilution, Sigma), goat anti-mouse HRP conjugated antibody (1:20000 dilution, Thermo Scientific) and goat anti-rabbit HRP conjugated antibody (1:20000 dilution, Thermo Scientific) were used to probe the membrane. SuperSignal West Pico chemiluminescent substrate (Thermo Scientific) was added to the membranes and chemiluminescent signals were revealed on X-ray films.

2D-DIGE analysis. The analysis was performed as previously described (Pescher et al, 2011). Briefly, 50 µg of G-Dye-labeled total protein extracts from wild-type and *cyp40-/-* promastigotes from stationary growth phase were separated in the first dimension by IEF on 18 cm pH 4 to 7 IPG strips, and the second dimension by SDS-PAGE. Three gels representing independent experimental replicates were scanned with a Typhoon imager and analyzed with the DeCyder^{TM} software package from GE Healthcare. Gels were stained with Lava purple, revealed by scanning on a Typhoon imager, and differentially expressed proteins were subjected to MS analysis.

Statistical analysis. Numerical data were expressed as mean ± standard deviation. Mann-Whitney U test was used to compare the significance between specific groups and $p < 0.05$ was considered as statistically significant. All statistical analysis was performed using either Excel 2003 (Microsoft) or Prism 5.0 (GraphPad).

Acknowledgments

We thank Dirk Schmidt-Arras (University of Kiel), Gabi Ommen, Mareike Chrobak and Christel Schmetz (Bernhard Nocht Institute, Hamburg) for discussion, Eric Prina for critical reading of the manuscript, Claire Forestier and Evie Melanitou (Institut Pasteur) for advices on macrophage experiment, Emanuelle Perret from the Institut Pasteur Imaging platform for advice on fluorescence microscopy, and Abdelkader Namane, Pascal Normand, and Christine Laurent from the Institut Pasteur Proteomics platform for protein determination and quantitative analysis of the 2D-DIGE gels. This work was supported by the Institut Pasteur, Réseau International des Instituts Pasteur, Centre Nationale de Recherche Scientifique, the 7th Framework Programme of the European Commission through a grant to the LEISHDRUG Project (223414), the Fondation de Médicale Recherche and Deutscher Akademischer Austausch Dienst, and the French Government's Investissements d'Avenir program: Laboratoire d'Excellence 'Integrative Biology of Emerging Infectious Diseases' (grant no. ANR-10-LABX-62-IBEID).

Figure legends

Fig 1. *L. donovani* CyP40 is a conserved chaperone and shows amastigote-specific phosphorylation. *(A) Amino acid sequence analysis of Leishmania CyP40.* Multiple alignment of CyP40 amino acid sequences of mammal (human, mouse and bovine), trypanosomatid (*Leishmania* and *Trypanosoma*) and yeast was performed using ClustalW as described in experimental procedures. CLD/PPIase (cyclophilin-like domain/PPIase) and TPR domains are indicated. Degree of residue conservation is represented by the colour code (green, 80-100% conserved; yellow, 30-80% conserved; red, 10-30% conserved). *, key residues for cyclosporin A binding and PPIase activity; ^, key residues for chaperone function; Δ, key residues for

698 HSP90 binding. Accession numbers: M.mus, NP_080628.1; H.sap, NP_005029.1; B. tau,
699 NP_776578.1; S.cer, NP_013317.1; T.cru, TcCLB.506885.400; T.bru, Tb927.9.9780; L.bra,
700 LbrM34.4730; L.mex, LmxM34.4770; L.inf, LinJ35.4830; L.maj, LmjF35.4770. *(B) Western*
701 *blot analysis.* Phosphoproteins of *in vitro* cultivated *L. donovani* promastigote (pro), axenic
702 amastigote (ax. ama, ax), and amastigotes harvested from infected hamster spleen (sp) were
703 enriched using a Phosphoprotein purification kit (Qiagen). Total and phosphoprotein extracts
704 were analyzed by Western blotting using anti-CyP40 antiserum and anti-α-tubulin antibody for
705 normalization.
706
707 **Fig. 2. CyP40 null mutant parasites are viable in culture.** *(A) Targeted replacement and*
708 *add-back strategies.* Targeting constructs comprising bleomycin (*BLE*) and puromycin (*PAC*)
709 resistance genes flanked by the *CYP40* 5' and 3' untranslated regions (UTRs) were used for
710 deletion of the genomic *CYP40* alleles. A targeting construct containing the nourseothricin
711 resistance gene (*SAT*) and the *Leishmania major CYP40* open reading frame (ORF) flanked by
712 the *L. major* small ribosomal subunit homology regions (*LmSSU*) were used for restoring
713 CyP40 expression in the *cyp40-/-* parasites. Primers specific for amplifying *CYP40* (P1/P4), the
714 resistance genes *PAC* (P2/P4) and *BLE* (P3/P4), and the *SSU* locus (P1/P5) are indicated. *(B)*
715 *Validation of homologous recombination events by PCR analysis.* Genomic DNA of wild-type
716 (WT), heterozygous CyP40 null mutant (-/+), homozygous CyP40 null mutant (-/-) and CyP40
717 add-back (-/-/+) was subjected to diagnostic PCR analysis using the indicated primer pairs
718 (P_xP_y) to amplify the endogenous CyP40 ORF (*CYP*), the *CYP40* ORF integrated into the
719 ribosomal locus (*SSU*), and the bleomycin (*BLE*) and puromycin (*PAC*) resistance genes. *(C)*
720 *Western blot analysis.* Total protein from wild-type (WT) and CyP40 null mutant (-/-) and add-
721 back (-/-/+) were extracted and analyzed by western blotting using anti-CyP40 (CyP, upper

722 panel) and anti-α-tubulin antibodies (Tub, lower panel). The molecular weight of marker
723 proteins in kDa is indicated.
724
725 **Fig. 3. Stationary *cyp40-/-* promastigotes show altered morphology.** *(A, B) Electron*
726 *microscopy analysis*. Promastigotes from stationary growth phase were fixed and processed for
727 either scanning (A) or transmission EM (B) as described in Materials and Methods. Scale bar
728 represents 10 μm in the scanning EM panels and 500 nm in the transmission EM panels. n,
729 nucleus; m, mitochondria; k, kinetoplast; f, flagellum; fp, flagellar pocket; l, lipid droplet. *(C)*
730 *Cell viability determination.* Stationary promastigotes of wild-type (WT) and *cyp40-/-* (-/-)
731 from 6 days cultures were stained with propidium iodide (PI, 1 μg/ml) and annexin V-FITC (1
732 μg/ml) for 10 min, and respective fluorescence intensities were analyzed by FACS. Numbers at
733 the lower-right quadrant represent percentage of apoptotic cells (PI-, Annexin V-FITC+), while
734 numbers at the upper-right quadrant represent percentage of dead cells (PI+, Annexin V-
735 FITC+).
736
737 **Fig 4. Growth characterization of Cyp40 null mutant promastigotes.** *(A) In vitro growth*
738 *curve of cyp40-/- mutants.* Promastigotes of wild-type (WT), *cyp40-*/- (-/-) and *cyp40-*/-/+ (-/-/+)
739 were cultured at 25ºC, pH 7.4 for 120 hours. Aliquots of culture were collected every 24 hours
740 and cell density was measured with a CASY cell counter. *(B) Western blot analysis of LPG*
741 *expression.* 5×10^6 wild-type or *cyp40-/-* parasites from logarithmic (log) or stationary (stat)
742 cell culture were subjected to western blot analysis using anti-LPG antibody. *(C) RT-PCR of*
743 *SHERP expression.* Total RNA of the wild-type (black), cyp40-/- (white) and cyp40-/-/+ (gray)
744 were extracted, reverse transcribed, and amplified with SHERP specific primer. β-tubulin was
745 amplified with specific primers as reference gene. Relative expression levels of SHERP mRNA
746 was analyzed using semi-quantitative RT-PCR.

747

748 **Fig. 5. Analyses of motility and cytoskeleton of stationary phase *cyp40-/-* promastigote.** *(A,*
749 *B) Motility analysis.* Motility tracks were established for logarithmic (log) and stationary phase
750 (stat) wild-type (WT), *cyp40-/-* (-/-) and *cyp40-/-/+* (-/-/+) promastigotes. For each condition, at
751 least 3 movies were recorded for the simultaneous *in silico* tracking of at least 255 cells per
752 movie. Mean speed (in μm/s) was calculated from instant velocity data and graphically
753 represented in left panel with SD bars. *ANOVA test, $p < 0.0001$. n=735 for WT Log and 737
754 for WT Stat, n=746 for -/- Log and 747 for -/- Stat, n=741 for -/-/+ Log and 742 for -/-/+ Stat.
755 Characteristic tracks are shown in Fig. 5B. *(C) Flagellar ultrastructure of stationary WT and*
756 *cyp40-/- promastigotes*. Scale bar represents 100 nm. *(D) Cytoskeleton analysis.* Wild-type
757 (WT) and *cyp40-/-* (-/-) stationary promastigotes were treated with 1% Triton X-100 at 4°C in
758 PBS for 10 minutes to strip the plasma membrane and visualize the parasite cytoskeleton.
759 Samples were washed twice in PBS, fixed and processed for scanning electron microscopy as
760 described (Absalon *et al*., 2008). Scale bar represents 100 nm. *(D) 2D-DIGE analysis.* The
761 readout of the DeCyder Biological Variation Analysis (BVA) module is shown for a small β-
762 tubulin isoform that shows four-fold reduced abundance in the null mutant abundance. The
763 upper panels represent 3D images of the volumes of the spots from wild-type (WT) and *cyp40-*
764 */-* (-/-). The bottom panel shows a graphic representation of differences in abundance across
765 three independent experiments. The numbers indicate the fold difference in abundance of
766 *cyp40-/-* to WT.

767

768 **Fig. 6. Intracellular survival and axenic differentiation of the *cyp40-/-* null mutants.** *(A)*
769 *Macrophage infection assay.* BMMs from C57BL/6 mice were infected with stationary phase
770 promastigotes of *L. donovani* wild-type (WT, ○), *cyp40-/-* (clone 4, □, and 5, ■) or *cyp40-/-/+*
771 (Δ) for 2 hours, and parasite burden was analyzed at 0, 24 and 48 hours post-infection by

772 nuclear staining with Hoechst 33342 and fluorescence microscopy. Results are representative
773 of three triplicate experiments with standard deviation denoted by the bars is shown. *(B)* In
774 vitro *growth curve of cyp40-/- axenic amastigotes.* Promastigotes of wild-type (WT), *cyp40*-/-
775 (-/-) and *cyp40*-/-/+ (-/-/+) were induced for axenic differentiation at 37ºC, pH 5.5 for 72 hours,
776 and amastigote growth was monitored following inoculation of 2×10^6 axenic amastigotes into
777 fresh medium and daily determination of cell density with a CASY cell counter. *(C) A2 marker*
778 *protein expression analysis.* Extracts from wild-type (WT), *cyp40*-/- (-/-) and *cyp40*-/-/+ (-/-/+)
779 axenic amastigotes 72 hours after incubation under differentiation-inducing conditions were
780 subjected to western blot analysis using an axenic amastigote marker A2-specific monoclonal
781 antibody (upper panel). Equal loading was controlled by Coomassie staining of an acrylamide
782 gel loaded with equivalent quantity of the samples (lower panel). The molecular weight of
783 marker proteins in kDa is indicated.
784
785 **Fig 7. Effect of phosphorylation of CyP40 on *Leishmania* intracellular survival.** *(A, B)*
786 *Phosphorylation site identification. (A)* Peptide 270LQQWSEAR277 (m/z 1098.49) was
787 identified in LC-ESI-MS/MS analysis of *L. major* Strep::CyP40 peptides after tryptic digestion
788 and TiO_2 enrichment and Ser274 was identified as a phosphorylated residue. *, fragment ions
789 arising from loss of ammonia (-17 Da); pS, phosphorylated serine. *(B) Multiple sequence*
790 *alignment of L. major CyP40 phospho-residue.* Sequence segments encompassing CyP40
791 phosphorylation site of mouse, human, bovine, yeast, two *Trypanosoma* (*T. cruzi*, *T. brucei*),
792 four *Leishmania* species (*L. braziliensis*, *L. mexicana*, *L. infantum*, *L. major*) were analyzed
793 with ClustalW. The phospho-residue Ser274 of *L. major* CyP40 is marked by an asterisk (*).
794 *(C) Analysis of the CyP40-S274A add-back line by western blotting.* Total protein (left panel)
795 from wild-type (WT), CyP40 null mutant (-/-) , CyP40 add-back lines Cyp40-WT and CyP40-
796 S274A (-/-/+ and S274A, respectively), and enriched phosphoprotein extracts (right panel) of

axenic amastigotes of *L. donovani* wild-type (WT) and *cyp40-/-/+S274A* (S274A) were analyzed. As background control of the phosphoprotein enrichment, 2 mg of the WT total extract were first treated with 8000 units of lambda phosphatase (ΛPP) for 2 hours at 30°C. The ΛPP-treated sample was then subjected to phosphoprotein enrichment. The total and phosphoprotein (Phospho) extracts of the parasites were analyzed by Western blotting using anti-CyP40 antiserum and anti-α-tubulin antibody. The molecular weight of marker proteins in kDa is indicated. *(D) Macrophage infection assay.* BMMs from C57BL/6 mice were infected for 2 hours with stationary phase promastigotes of *L. donovani* wild-type (WT, O), *cyp40-/-* (-/-, □) or CyP40-WT and CyP40-S274A add-backs (respectively -/-/+, Δ and -/-/+S/A, ▼) and parasite burden was at 0, 24 and 48 hours post-infection by nuclear staining with Hoechst 33342 and fluorescence microscopy. Result is presented as percentage infected BMMs (left panel, one representative triplicate experiment with standard deviation denoted by the bars is shown), and number of parasites per 100 BMMs at 48 hours post-infection (right panels, results of one representative triplicate experiment with standard deviation denoted by the bars is shown).

References

Absalon, S., Blisnick, T., Bonhivers, M., Kohl, L., Cayet, N., Toutirais, G., *et al.* (2008) Flagellum elongation is required for correct structure, orientation and function of the flagellar pocket in *Trypanosoma brucei*. *J Cell Sci* **121:** 3704-3716.

Barak, E., Amin-Spector, S., Gerliak, E., Goyard, S., Holland, N. and Zilberstein, D. (2005) Differentiation of *Leishmania donovani* in host-free system: analysis of signal perception and response. *Mol Biochem Parasitol* **141:** 99-108.

822 Barik, S. (2006) Immunophilins: for the love of proteins. *Cell Mol Life Sci* **63:** 2889-2900.

823 Bates, P.A., and Tetley, L. (1993) *Leishmania mexicana*: Induction of metacyclogenesis by
824 cultivation of promastigotes at acidic pH. *Exp Parasitol* **76:** 412–423.

825 Brasseur, A., Rotureau, B., Vermeersch, M., Blisnick, T., Salmon, D., Bastin, P., Pays, E.,
826 Vanhamme, L., and Pérez-Morga, D. (2013) *Trypanosoma brucei* FKBP12 differentially
827 controls motility and cytokinesis in procyclic and bloodstream forms. *Euk Cell* **12:** 168–181.

828 Chambraud, B., Belabes, H., Fontaine-Lenoir, V., Fellous, A. and Baulieu, E.E. (2007) The
829 immunophilin FKBP52 specifically binds to tubulin and prevents microtubule formation.
830 *FASEB J* **21:** 2787-2797.

831 Chappell, L.H. and Wastling, J.M. (1992) Cyclosporin A: antiparasite drug, modulator of the
832 host-parasite relationship and immunosuppressant. *Parasitology* **105 Suppl:** S25-40.

833 Cunningham, M.L., Titus, R.G., Turco, S.J. and Beverley, S.M. (2001) Regulation of
834 differentiation to the infective stage of the protozoan parasite *Leishmania major* by
835 tetrahydrobiopterin. *Science* **292:** 285-287.

836 da Silva, R. and Sacks, D.L. (1987) Metacyclogenesis is a major determinant of *Leishmania*
837 promastigote virulence and attenuation. *Infect Immun* **55:** 2802-2806.

838 Drummelsmith, J., Brochu, V., Girard, I., Messier, N. and Ouellette, M. (2003) Proteome
839 mapping of the protozoan parasite *Leishmania* and application to the study of drug targets
840 and resistance mechanisms. *Mol Cell Proteomics* **2:** 146-155.

841 Duina, A.A., Marsh, J.A. and Gaber, R.F. (1996) Identification of two CyP-40-like cyclophilins
842 in *Saccharomyces cerevisiae*, one of which is required for normal growth. *Yeast* **12:** 943-952.

843 Forestier, C.L., Machu, C., Loussert, C., Pescher, P. and Spath, G.F. (2011) Imaging host cell-
844 *Leishmania* interaction dynamics implicates parasite motility, lysosome recruitment, and
845 host cell wounding in the infection process. *Cell Host Microbe* **9:** 319-330.

846 Galigniana, M.D., Radanyi, C., Renoir, J.M., Housley, P.R., and Pratt, W.B. (2001) Evidence
847 that the peptidylprolyl isomerase domain of the hsp90-binding immunophilin FKBP52 is
848 involved in both dynein interaction and glucocorticoid receptor movement to the nucleus. *J*
849 *Biol Chem* **276:** 14884–14889.
850 Galigniana, M.D., Morishima, Y., Gallay, P.A., and Pratt, W.B. (2004) Cyclophilin-A is bound
851 through its peptidylprolyl isomerase domain to the cytoplasmic dynein motor protein
852 complex. *J Biol Chem* **279:** 55754–55759.
853 Gannavaram, S., and Debrabant, A. (2012) Programmed cell death in *Leishmania*: biochemical
854 evidence and role in parasite infectivity. *Front Cell Infect Microbiol* **2:** 95.
855 Goyard, S., Segawa, H., Gordon, J., Showalter, M., Duncan, R., Turco, S.J. and Beverley, S.M.
856 (2003) An *in vitro* system for developmental and genetic studies of *Leishmania donovani*
857 phosphoglycans. *Mol Biochem Parasitol* **130:** 31-42.
858 Hem, S., Gherardini, P.F., Osorio y Fortea, J., Hourdel, V., Morales, M.A., Watanabe, R.*, et al.*
859 (2010) Identification of *Leishmania*-specific protein phosphorylation sites by LC-MS/MS
860 and comparative genomics analyses. *Proteomics* **10:** 3868-3883.
861 Henikoff, S., and Henikoff, J.G. (1993) Performance evaluation of amino acid substitution
862 matrices. *Proteins* **17:** 49–61.
863 Hoffmann, K. and Handschumacher, R.E. (1995) Cyclophilin-40: evidence for a dimeric
864 complex with hsp90. *Biochem J* **307:** 5-8.
865 Hombach, A., Ommen, G., Chrobak, M., and Clos, J. (2012) The Hsp90-Sti1 Interaction is
866 Critical for Leishmania donovani Proliferation in Both Life Cycle Stages. *Cell Microbiol*
867 (Epub ahead of print)
868 Hong, J., Kim, S.T., Tranguch, S., Smith, D.F., and Dey, S.K. (2007) Deficiency of co-
869 chaperone immunophilin FKBP52 compromises sperm fertilizing capacity. *Reproduction*
870 **133:** 395–403.

871 Hoyer, C., Zander, D., Fleischer, S., Schilhabel, M., Kroener, M., Platzer, M. and Clos, J. (2004)
872 A *Leishmania donovani* gene that confers accelerated recovery from stationary phase growth
873 arrest. *Int J Parasitol* **34:** 803-811.
874 Hubel, A., Krobitsch, S., Horauf, A. and Clos, J. (1997) *Leishmania major* Hsp100 is required
875 chiefly in the mammalian stage of the parasite. *Mol Cell Biol* **17:** 5987 - 5995.
876 IIki, T., Yoshikawa, M., Meshi, T., and Ishikawa, M. (2012) Cyclophilin 40 facilitates HSP90-
877 mediated RISC assembly in plants. *EMBO J* **31:** 267–278.
878 Kapler, G.M., Coburn, C.M. and Beverley, S.M. (1990) Stable transfection of the human
879 parasite *Leishmania major* delineates a 30-kilobase region sufficient for extrachromosomal
880 replication and expression. *Mol Cell Biol* **10:** 1084-1094.
881 Kearse, M., Moir, R., Wilson, A., Stones-Havas, S., Cheung, M., Sturrock, S., Buxton, S.,
882 Cooper, A., Markowitz, S., Duran, C., et al. (2012) Geneious Basic: an integrated and
883 extendable desktop software platform for the organization and analysis of sequence data.
884 *Bioinformatics* **28:** 1647–1649.
885 Krobitsch, S., and Clos, J. (1999) A novel role for 100 kD heat shock proteins in the parasite
886 *Leishmania donovani*. *Cell Stress Chaperones* **4:** 191–198.
887 Kulkarni, M.M., Karafova, A., Kamysz, W., Schenkman, S., Pelle, R., and McGwire, B.S.
888 (2013) Secreted trypanosome cyclophilin inactivates lytic insect defense peptides and
889 induces parasite calcineurin activation and infectivity. *J Biol Chem* **288:** 8772–8784.
890 Larkin, M.A., Blackshields, G., Brown, N.P., Chenna, R., McGettigan, P.A., McWilliam, H.,
891 Valentin, F., Wallace, I.M., Wilm, A., Lopez, R., et al. (2007) Clustal W and Clustal X
892 version 2.0. *Bioinformatics* **23:** 2947–2948.
893 Laubach, V.E., Shesely, E.G., Smithies, O. and Sherman, P.A. (1995) Mice lacking inducible
894 nitric oxide synthase are not resistant to lipopolysaccharide-induced death. *Proc Natl Acad*
895 *Sci U S A* **92:** 10688-10692.

896 Lee, N., Bertholet, S., Debrabant, A., Muller, J., Duncan, R., and Nakhasi, H.L. (2002)
897 Programmed cell death in the unicellular protozoan parasite *Leishmania*. *Cell Death Differ*
898 **9:** 53–64.
899 Li, J., Richter, K. and Buchner, J. (2011) Mixed Hsp90-cochaperone complexes are important
900 for the progression of the reaction cycle. *Nat Struct Mol Biol* **18:** 61-66.
901 Mark, P.J., Ward, B.K., Kumar, P., Lahooti, H., Minchin, R.F. and Ratajczak, T. (2001) Human
902 cyclophilin 40 is a heat shock protein that exhibits altered intracellular localization
903 following heat shock. *Cell Stress Chaperones* **6:** 59-70.
904 Miyata, Y., Chambraud, B., Radanyi, C., Leclerc, J., Lebeau, M.C., Renoir, J.M., Shirai, R.,
905 Catelli, M.G., Yahara, I., and Baulieu, E.E. (1997) Phosphorylation of the
906 immunosuppressant FK506-binding protein FKBP52 by casein kinase II: regulation of
907 HSP90-binding activity of FKBP52. *Proc Natl Acad Sci U S A* **94:** 14500–14505.
908 Mojtahedi, Z., Clos, J. and Kamali-Sarvestani, E. (2008) *Leishmania major*: Identification of
909 developmentally regulated proteins in procyclic and metacyclic promastigotes. *Exp*
910 *Parasitol* **119:** 422-429.
911 Mok, D., Allan, R.K., Carrello, A., Wangoo, K., Walkinshaw, M.D., and Ratajczak, T. (2006)
912 The chaperone function of cyclophilin 40 maps to a cleft between the prolyl isomerase and
913 tetratricopeptide repeat domains. *FEBS Lett* **580:** 2761–2768.
914 Morales, M.A., Renaud, O., Faigle, W., Shorte, S.L. and Spath, G.F. (2007) Over-expression of
915 *Leishmania major* MAP kinases reveals stage-specific induction of phosphotransferase
916 activity. *Int J Parasitol* **37:** 1187-1199.
917 Morales, M.A., Watanabe, R., Laurent, C., Lenormand, P., Rousselle, J.C., Namane, A. and
918 Spath, G.F. (2008) Phosphoproteomic analysis of *Leishmania donovani* pro- and amastigote
919 stages. *Proteomics* **8:** 350-363.

Morales, M.A., Watanabe, R., Dacher, M., Chafey, P., Osorio y Fortea, J., Scott, D.A., *et al.* (2010) Phosphoproteome dynamics reveal heat-shock protein complexes specific to the *Leishmania donovani* infectious stage. *Proc Natl Acad Sci U S A* **107:** 8381-8386.

Oberholzer, M., Langousis, G., Nguyen, H.T., Saada, E.A., Shimogawa, M.M., Jonsson, Z.O., Nguyen, S.M., Wohlschlegel, J.A., and Hill, K.L. (2011) Independent analysis of the flagellum surface and matrix proteomes provides insight into flagellum signaling in mammalian-infectious *Trypanosoma brucei*. *Mol Cell Proteomics* **10:** M111.010538.

Ommen, G., Lorenz, S. and Clos, J. (2009) One-step generation of double-allele gene replacement mutants in *Leishmania donovani*. *Int J Parasitol* **39:** 541-546.

Parodi-Talice, A., Monteiro-Goes, V., Arrambide, N., Avila, A.R., Duran, R., Correa, A., *et al.* (2007) Proteomic analysis of metacyclic trypomastigotes undergoing *Trypanosoma cruzi* metacyclogenesis. *J Mass Spectrom* **42:** 1422-1432.

Pearl, L.H., and Prodromou, C. (2000) Structure and *in vivo* function of Hsp90. *Curr Opin Struct Biol* **10:** 46–51.

Pearl, L.H., and Prodromou, C. (2006) Structure and mechanism of the Hsp90 molecular chaperone machinery. *Annu Rev Biochem* **75:** 271–294.

Pescher, P., Blisnick, T., Bastin, P., and Spath, G.F. (2011) Quantitative proteome profiling informs on phenotypic traits that adapt *Leishmania donovani* for axenic and intracellular proliferation. *Cell Microbiol* **13:** 978–991.

Pollock, J.D., Williams, D.A., Gifford, M.A., Li, L.L., Du, X., Fisherman, J., *et al.* (1995) Mouse model of X-linked chronic granulomatous disease, an inherited defect in phagocyte superoxide production. *Nat Genet* **9:** 202-209.

Pratt, W.B., and Dittmar, K.D. (1998) Studies with purified chaperones advance the understanding of the mechanism of glucocorticoid receptor-hsp90 heterocomplex assembly. *Trends Endocrinol Metab* **9:** 244–252.

945 Pratt, W.B., Galigniana, M.D., Harrell, J.M. and DeFranco, D.B. (2004) Role of hsp90 and the
946 hsp90-binding immunophilins in signalling protein movement. *Cell Signal* **16:** 857-872.
947 Ratajczak, T., Ward, B.K., and Minchin, R.F. (2003) Immunophilin chaperones in steroid
948 receptor signalling. *Curr Top Med Chem* **3:** 1348–1357.
949 Ratajczak, T., Ward, B.K., Cluning, C. and Allan, R.K. (2009) Cyclophilin 40: An Hsp90-
950 cochaperone associated with apo-steroid receptors. *Int J Biochem Cell Biol* **41:** 1652-1655.
951 Riggs, D.L., Cox, M.B., Cheung-Flynn, J., Prapapanich, V., Carrigan, P.E., and Smith, D.F.
952 (2004) Functional specificity of co-chaperone interactions with Hsp90 client proteins. *Crit*
953 *Rev Biochem Mol Biol* **39:** 279–295.
954 Rosenzweig, D., Smith, D., Opperdoes, F., Stern, S., Olafson, R.W. and Zilberstein, D. (2008)
955 Retooling *Leishmania* metabolism: from sand fly gut to human macrophage. *FASEB J* **22:**
956 590-602.
957 Sacks, D.L. and Perkins, P.V. (1984) Identification of an infective stage of *Leishmania*
958 promastigotes. *Science* **223:** 1417-1419.
959 Seeback, T., Hemphill, A., and Lawson, D. (1990) The cytoskeleton of trypanosomes.
960 *Parasitol Today* **6:** 49–52.
961 Serafim, T.D., Figueiredo, A.B., Costa, P.A.C., Marques-da-Silva, E.A., Gonçalves, R., de
962 Moura, S.A.L., Gontijo, N.F., da Silva, S.M. et al. (2012) *Leishmania* metacyclogenesis is
963 promoted in the absence of purines. *PLoS Negl Trop Dis* **6:** e1833.
964 Silverman, J.M., Chan, S.K., Robinson, D.P., Dwyer, D.M., Nandan, D., Foster, L.J., and
965 Reiner, N.E. (2008) Proteomic analysis of the secretome of *Leishmania donovani*. *Genome*
966 *Biol* **9:** R35.
967 Silverman, J.M., Clos, J., Horakova, E., Wang, A.Y., Wiesgigl, M., Kelly, I., Lynn, M.A.,
968 McMaster, W.R., Foster, L.J., Levings, M.K., et al. (2010) *Leishmania* exosomes modulate

969 innate and adaptive immune responses through effects on monocytes and dendritic cells. *J*
970 *Immunol* **185:** 5011–5022.
971 Silverstein, A.M., Galigniana, M.D., Kanelakis, K.C., Radanyi, C., Renoir, J.M., and Pratt,
972 W.B. (1999) Different regions of the immunophilin FKBP52 determine its association with
973 the glucocorticoid receptor, hsp90, and cytoplasmic dynein. *J Biol Chem* **274:** 36980–36986.
974 Smith, M.R., Willmann, M.R., Wu, G., Berardini, T.Z., Möller, B., Weijers, D. and Poethig,
975 R.S. (2009) Cyclophilin 40 is required for microRNA activity in Arabidopsis. *Proc Natl*
976 *Acad Sci U S A* **106:** 5424-5429.
977 Spath, G.F., Epstein, L., Leader, B., Singer, S.M., Avila, H.A., Turco, S.J. and Beverley, S.M.
978 (2000) Lipophosphoglycan is a virulence factor distinct from related glycoconjugates in the
979 protozoan parasite *Leishmania major*. *Proc Natl Acad Sci U S A* **97:** 9258-9263.
980 Tolson, D.L., Schnur, L.F., Jardim, A. and Pearson, T.W. (1994) Distribution of
981 lipophosphoglycan-associated epitopes in different *Leishmania* species and in African
982 trypanosomes. *Parasitol Res* **8:** 537-542.
983 Uezato, H., Kato, H., Kayo, S., Hagiwara, K., Bhutto, A., Katakura, K., Nonaka, S., and
984 Hashiguchi, Y. (2005) The attachment and entry of *Leishmania* (*Leishmania*) *major* into
985 macrophages: observation by scanning electron microscope. *J Dermatol* **32:** 534–540.
986 Walczak, C.E. (2000) Microtubule dynamics and tubulin interacting proteins. *Curr Opin Cell*
987 *Biol* **12:** 52–56.
988 Walters, L.L., Modi, G.B., Chaplin, G.L., and Tesh, R.B. (1989) Ultrastructural development of
989 *Leishmania chagasi* in its vector, *Lutzomyia longipalpis* (Diptera: Psychodidae). *Am J Trop*
990 *Med Hyg* **41:** 295–317.
991 Walters, L.L., Irons, K.P., Chaplin, G., and Tesh, R.B. (1993) Life cycle of *Leishmania major*
992 (Kinetoplastida: Trypanosomatidae) in the neotropical sand fly *Lutzomyia longipalpis*
993 (Diptera: Psychodidae). *J Med Entomol* **30:** 699–718.

994 Ward, B.K., Allan, R.K., Mok, D., Temple, S.E., Taylor, P., Dornan, J et al. (2002) A structure-
995 based mutational analysis of cyclophilin 40 identifies key residues in the core
996 tetratricopeptide repeat domain that mediate binding to Hsp90. *J Biol Chem* **277:** 40799–
997 40809.
998 Warth, R., Briand, P.A. and Picard, D. (1997) Functional analysis of the yeast 40 kDa
999 cyclophilin Cyp40 and its role for viability and steroid receptor regulation. *Biol Chem* **378:**
1000 381-391.
1001 Weisman, R., Creanor, J. and Fantes, P. (1996) A multicopy suppressor of a cell cycle defect in
1002 *S. pombe* encodes a heat shock inducible 40 kDa cyclophilin-like protein. *EMBO J* **15:** 447-
1003 456.
1004 Wiesgigl, M. and Clos, J. (2001) Heat Shock Protein 90 Homeostasis Controls Stage
1005 Differentiation in Leishmania donovani. *Mol Biol Cell* **12:** 3307-3316.
1006 Yau, W.L., Blisnick, T., Taly, J.F., Helmer-Citterich, M., Schiene-Fischer, C., Leclercq, O.*, et*
1007 *al.* (2010) Cyclosporin A treatment of *Leishmania donovani* reveals stage-specific functions
1008 of cyclophilins in parasite proliferation and viability. *PLoS Negl Trop Dis* **4:** e729.
1009 Zakai, H.A., Chance, M.L. and Bates, P.A. (1998) *In vitro* stimulation of metacyclogenesis in
1010 *Leishmania braziliensis, L. donovani, L. major* and *L. mexicana*. *Parasitology* **116:** 305-309.
1011 Zhang, W.W., Charest, H., Ghedin, E. and Matlashewski, G. (1996) Identification and
1012 overexpression of the A2 amastigote-specific protein in *Leishmania donovani*. *Mol Biochem*
1013 *Parasitol* **78:** 79-90.
1014 Zilberstein, D. and Shapira, M. (1994) The role of pH and temperature in the development of
1015 *Leishmania* parasites. *Annu Rev Microbiol* **48:** 449-470.
1016
1017
1018

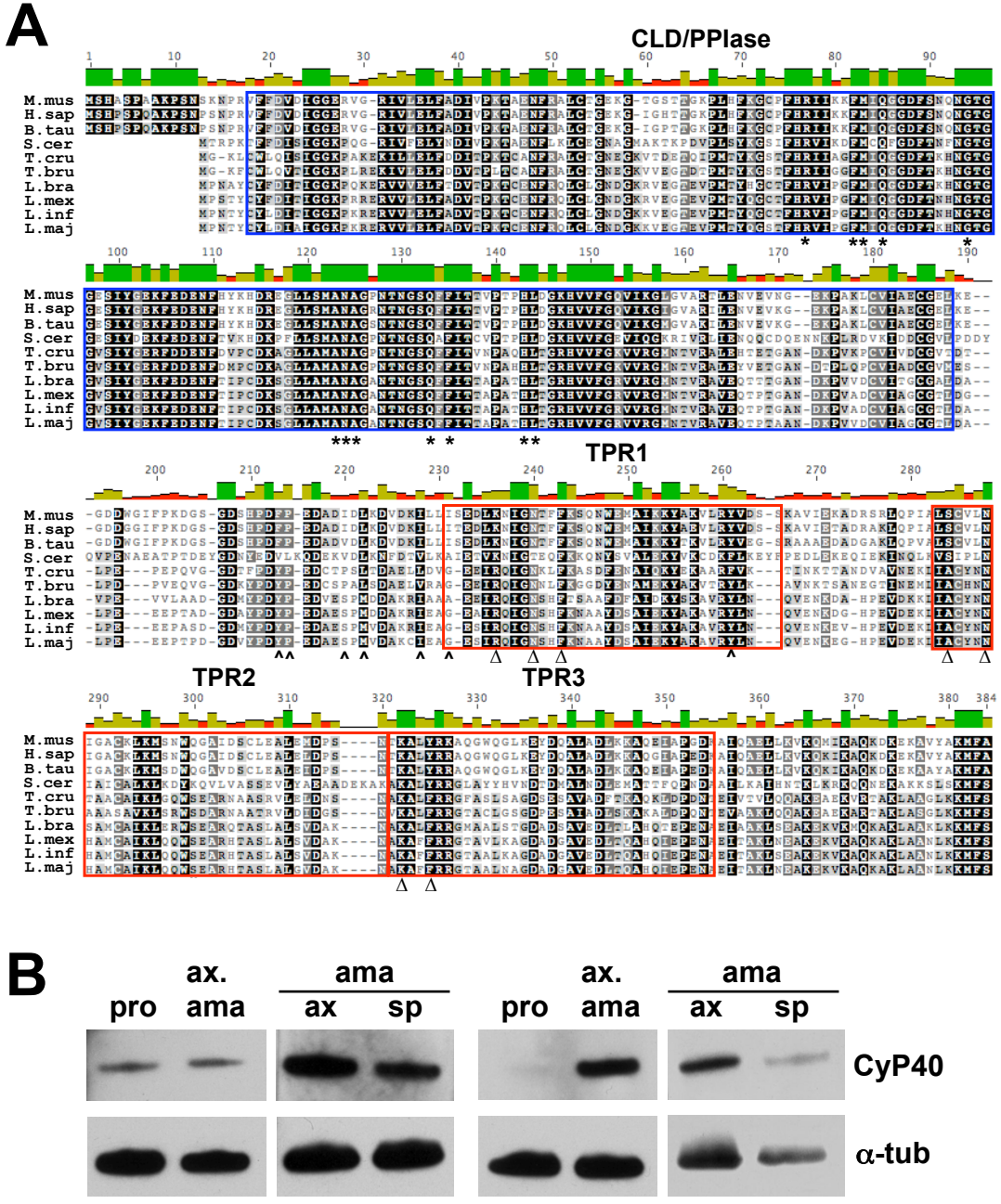
A
CLD/PPIase
TPR1
TPR2
TPR3
M.mus
H.sap
B.tau
S.cer
T.cru
T.bru
L.bra
L.mex
L.inf
L.maj
B
ax.
ama
pro
ama
ax
sp
CyP40
α-tub
total protein
phospho protein

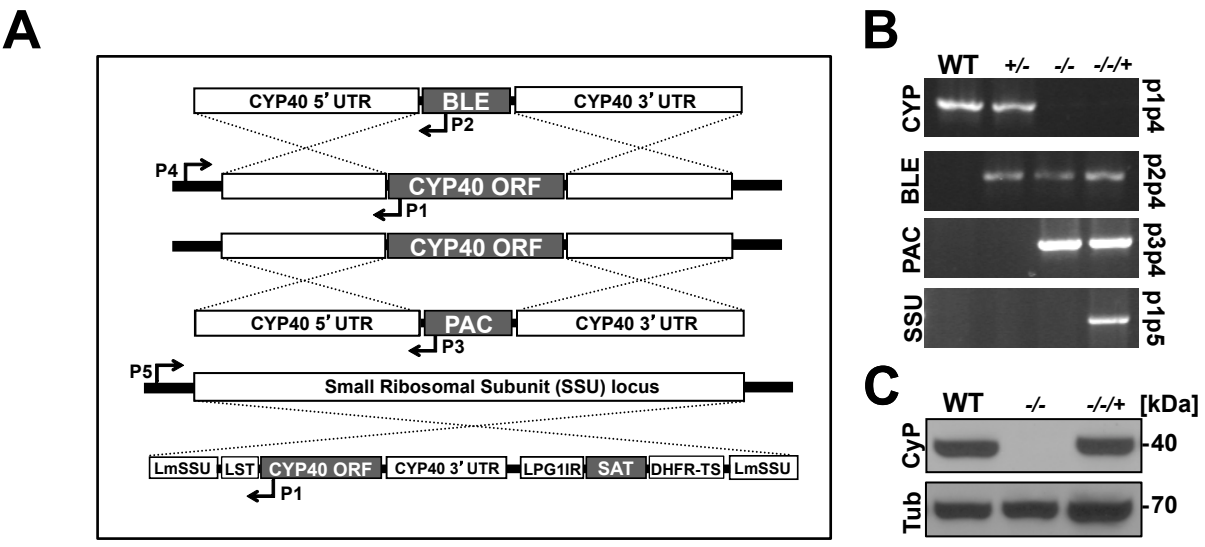
A
CYP40 5' UTR
BLE
CYP40 3' UTR
P2
P4
CYP40 ORF
P1
CYP40 ORF
CYP40 5' UTR
PAC
CYP40 3' UTR
P3
P5
Small Ribosomal Subunit (SSU) locus
LmSSU
LST
CYP40 ORF
CYP40 3' UTR
LPG1IR
SAT
DHFR-TS
LmSSU
P1
B
WT
+/-
-/-
-/-/+
CYP
p1p4
BLE
p2p4
PAC
p3p4
SSU
p1p5
C
WT
-/-
-/-/+
[kDa]
CyP
40
Tub
70

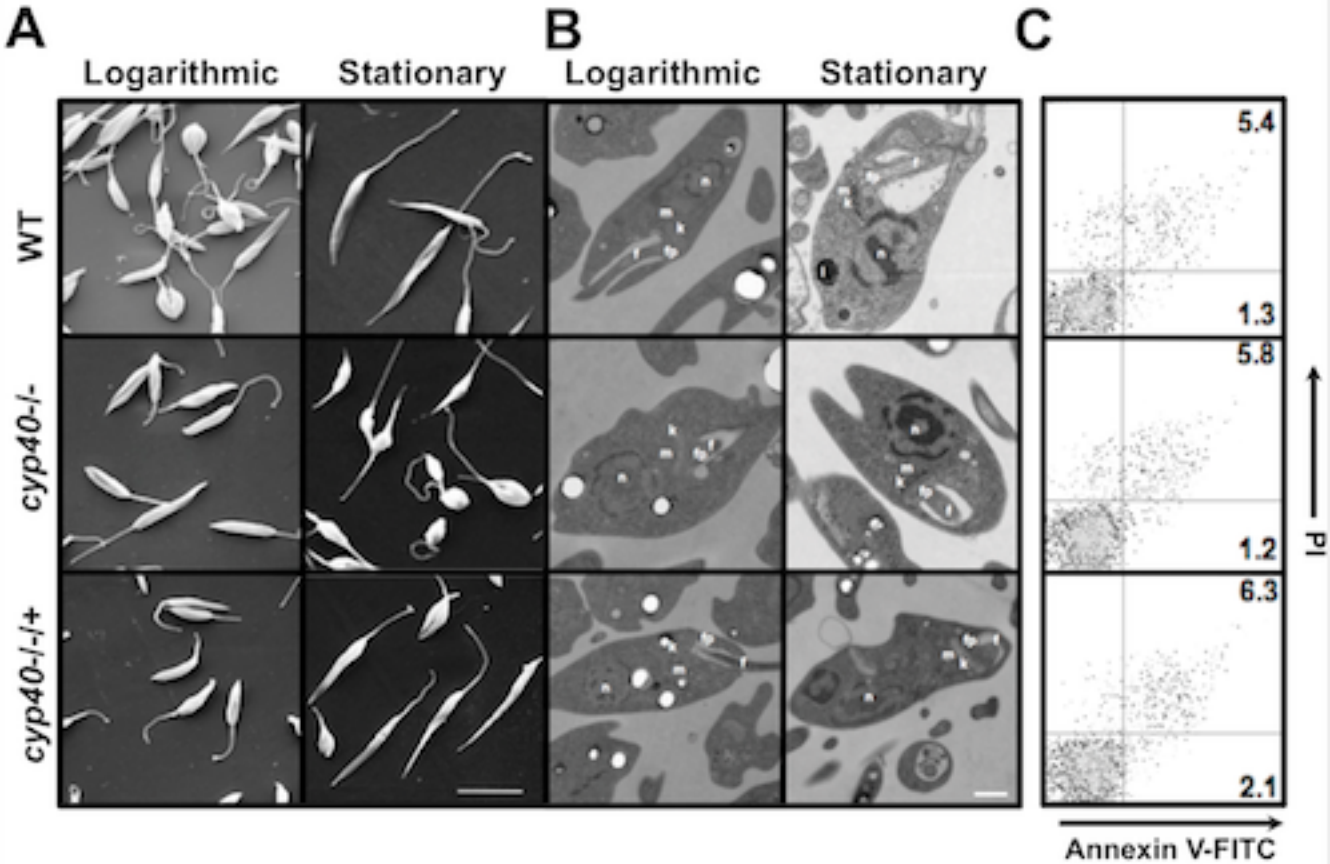
A
B
C
Logarithmic
Stationary
Logarithmic
Stationary
WT
cyp40-/-
cyp40-/-/+
5.4
1.3
5.8
1.2
6.3
2.1
PI
Annexin V-FITC

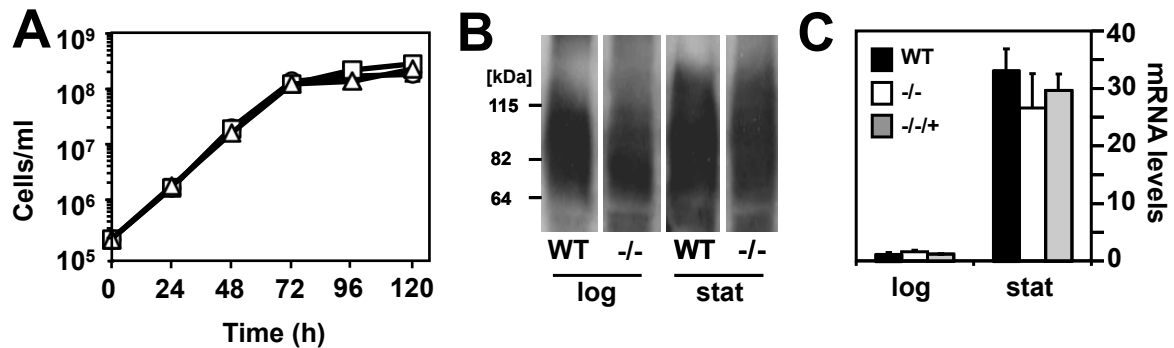
A
Cells/ml
10^9
10^8
10^7
10^6
10^5
0
24
48
72
96
120
Time (h)
B
[kDa]
115
82
64
WT
-/-
WT
-/-
log
stat
C
WT
-/-
-/-/+
mRNA levels
40
30
20
10
0
log
stat

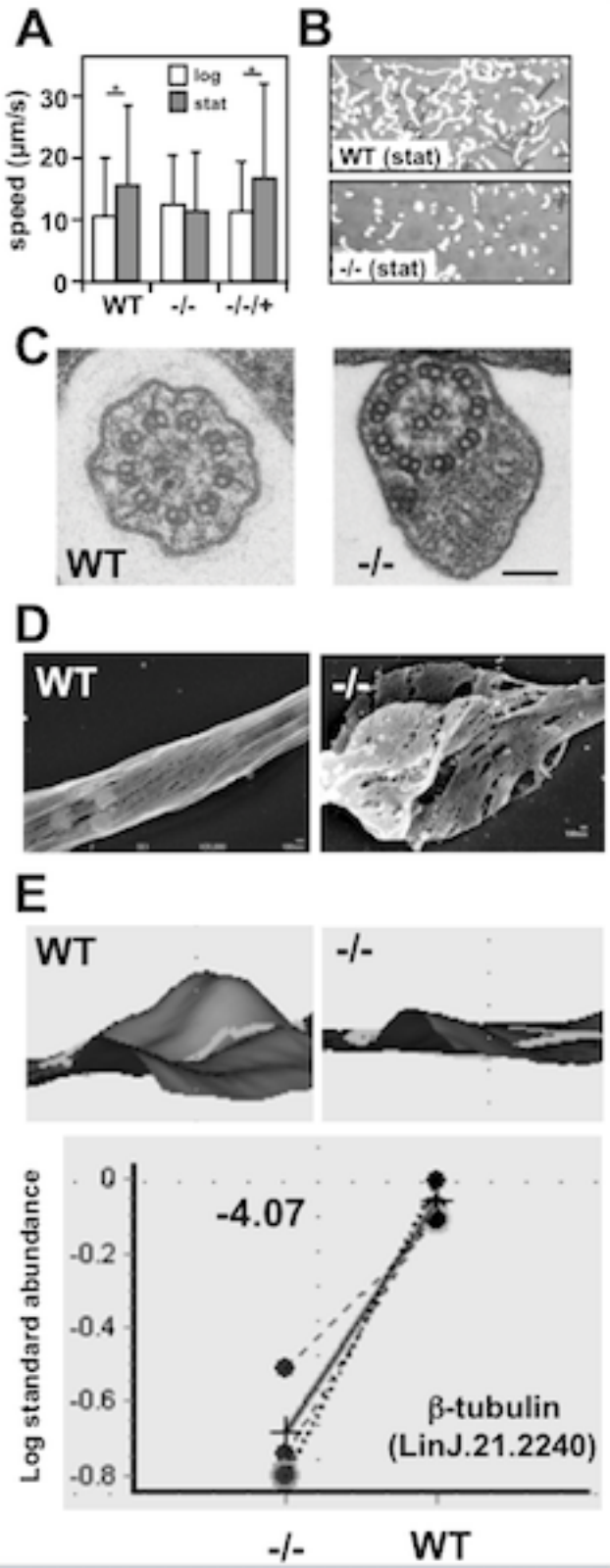
A
B
C
D
E
speed (μm/s)
log
stat
WT
-/-
-/-/+
WT (stat)
-/- (stat)
WT
-/-
WT
-/-
Log standard abundance
-4.07
β-tubulin
(LinJ.21.2240)
-/-
WT

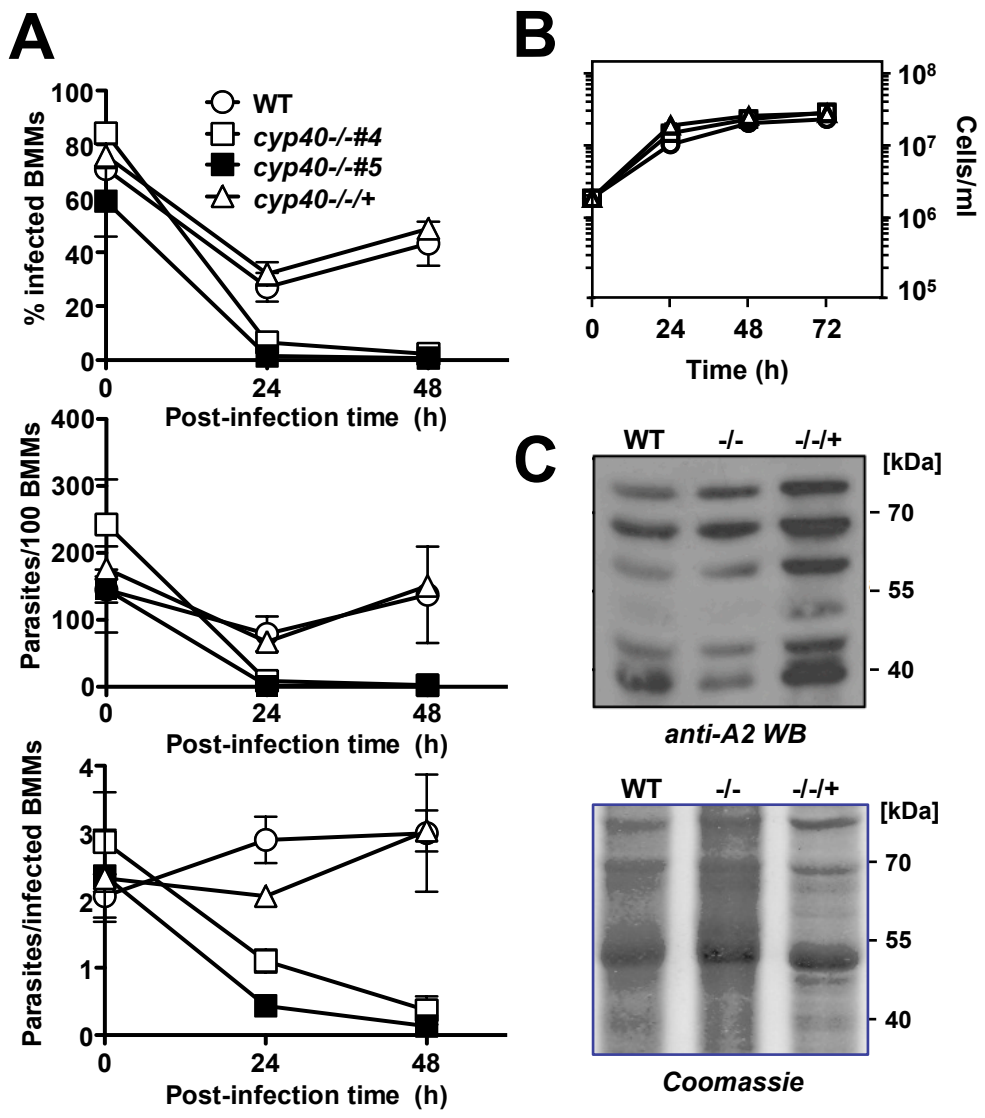
A
% infected BMMs
100
80
60
40
20
0
WT
cyp40-/-#4
cyp40-/-#5
cyp40-/-/+
0
24
48
Post-infection time (h)
Parasites/100 BMMs
400
300
200
100
0
0
24
48
Post-infection time (h)
Parasites/infected BMMs
4
3
2
1
0
0
24
48
Post-infection time (h)
B
Cells/ml
10^8
10^7
10^6
10^5
0
24
48
72
Time (h)
C
WT
-/-
-/-/+
[kDa]
70
55
40
anti-A2 WB
WT
-/-
-/-/+
[kDa]
70
55
40
Coomassie

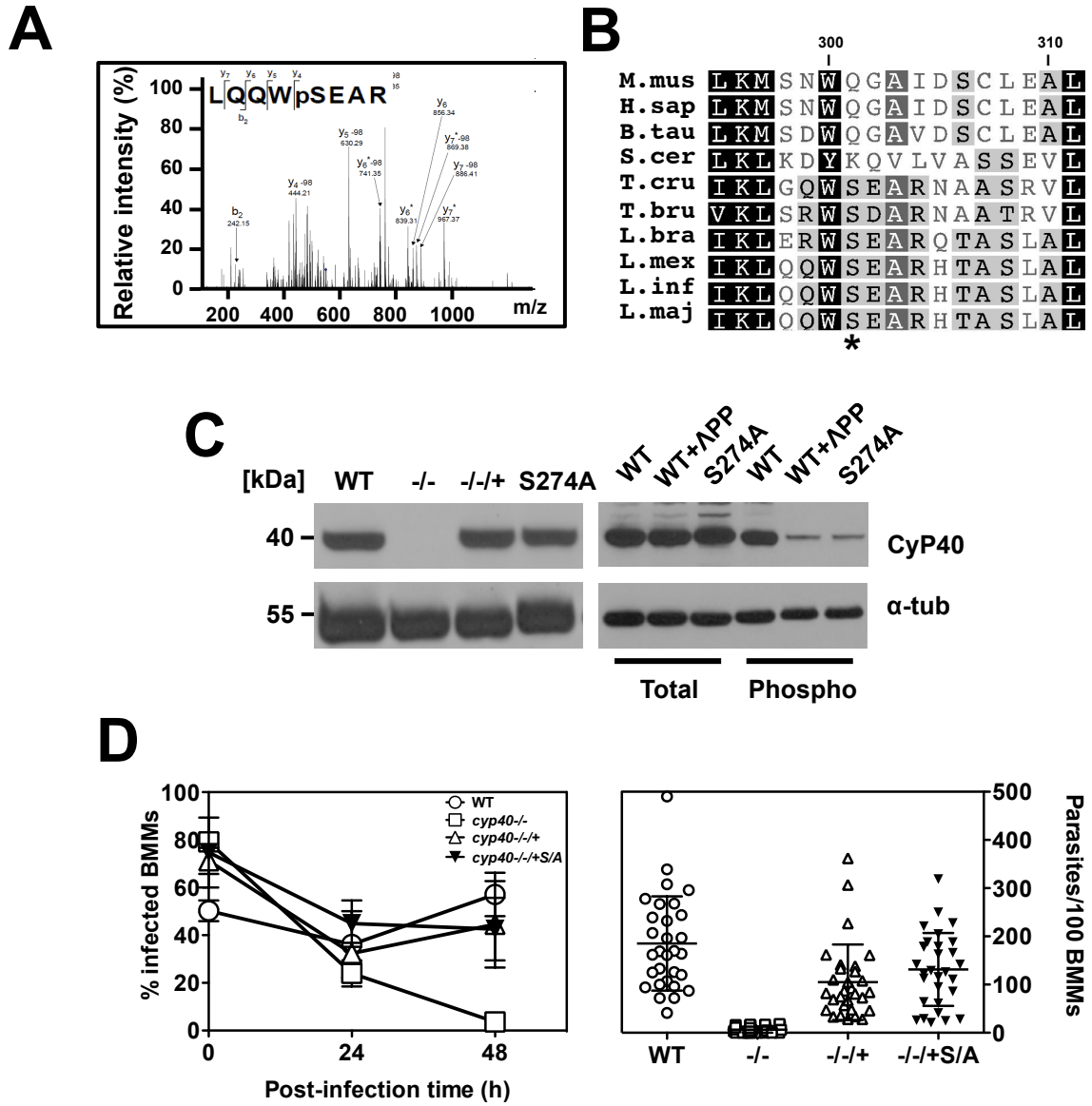
A
Relative intensity (%)
LQQWpSEAR
m/z
B
300
310
M.mus LKMSNWQGAIDSCLEAL
H.sap LKMSNWQGAIDSCLEAL
B.tau LKMSDWQGAVDSCLEAL
S.cer LKLKDYKQVLVASSEVL
T.cru IKLGQWSEARNAASRVL
T.bru VKLSRWSDARNAATRVL
L.bra IKLERWSEARQTASLAL
L.mex IKLQQWSEARHTASLAL
L.inf IKLQQWSEARHTASLAL
L.maj IKLQQWSEARHTASLAL
*
C
[kDa]
WT
-/-
-/-/+
S274A
WT
WT+APP
S274A
WT
WT+APP
S274A
40
55
CyP40
α-tub
Total
Phospho
D
% infected BMMs
Post-infection time (h)
WT
cyp40-/-
cyp40-/-/+
cyp40-/-/+S/A
Parasites/100 BMMs
WT
-/-
-/-/+
-/-/+S/A